UNIVERSITÀ POLITECNICA DELLE MARCHE

FACOLTÀ DI INGEGNERIA

Corso di Laurea Magistrale in Biomedical Engineering

A machine-learning approach to EMG-based classification of gait phases and sub-phases.

Relatore:
Prof. Lorenzo Scalise

Tesi di Laurea di:
Alessio Di Lello

Correlatore:
Prof. Francesco Di Nardo
Prof. Christian Morbidoni

Anno Accademico 2020/2021

Acknowledgments

For the development of this thesis, I would like to thank my supervisor Lorenzo Scalise and co-supervisors Francesco Di Nardo and Christian Morbidoni for their great help and for reviewing my manuscript. Moreover, I would strongly to thank my fellow students and especially great friends Federico Barbarossa, Giacomo Verde and Giacomo Covella for the support given each other in these fantastic five years. A big thank you to my family who have always been close to me in everything I have done beyond my studies.

Contents

1. Introduction

Human walking can be described as a cyclic pattern of body movements which moves forward an individual's position [1]. The human gait cycle can be divided in two main phases representing the period when the foot is in contact with the ground (Stance phase) and the period when the foot is in the air for limb advancement (Swing phase) [2]. The transition between a swing and the subsequent stance phase is commonly referred to as heel-strike (HS), while the transition between a stance and the subsequent swing phase is referred to as toe-off (TO). Identifying the gait events allows to quantify the duration of all gait phases and analyse the gait activity. The current gold standard method for the detection of gait events involves the use of ground reaction force (vertical projection of centre of pressure of the body) measured by force platforms [3]. However, this method present relevant issues: foot drugging during swing phase provokes false force thresholds diminishing the accuracy of detection. This issue can be avoided determining gait events manually, anyway, is a process highly variable, time consuming and depend on operator competence. These issues were overcome introducing a computational method for the automatic gait event detection based on cinematic data collected using physical sensors [3]. However, gait events detection using physical sensor produces unnatural gait behaviour and doesn't recognize enough the real subject's intention.

The human walking is controlled by the coordinated activities of several muscles of lower limb acting at hip, knee, and ankle, this means that gait phases can be deduced collecting information regarding muscle contraction with electromyographic signals. In particular, the surface electromyographic signals (sEMG) contain rich information about muscle excitation and are acquired on the surface of the muscle in a non-invasive way using surface electrodes [4]. Thus, surface electromyographic signals can be applied in several biomechanics studies, for instance, human gesture classification [5-6] or motion estimation [7], hence can be applied to recognize gait phases. In recent years, artificial-intelligence techniques have been proposed for the classification of stance vs. swing and for the assessment of HS and TO [8, 9]. Particularly valuable are those methodologies where machine and deep learning are implemented with the aim of limiting the number of sensors involved in the experimental set-up, such as electromyography-based approaches [9-15]. These studies are designed to classify gait phases and predict gait events from only surface electromyographic signals (sEMG), avoiding the requirement of directly measuring temporal data by means of additional systems or sensors (foot-switch sensors, IMUs, pressure mats, stereo-photogrammetry). This would allow to reduce burden for patient, simplify clinical protocols, and make test faster, specifically in the evaluation of neuromuscular diseases or for walking-aid devices

where the acquisition of myoelectric signals is largely advised [16, 17]. To our knowledge, best-performing results are achieved by the study proposed in [18].

However, the stance phase could be further split in three subphases [2]. During the first sub-phases, the body weight is supported by the limb in contact with the ground, then the body is led forward during the later stages of stance. The gait cycle is defined as a sequence of the following three sub-phases of stance: Heel Contact (HC), Flat foot Contact (FFC), Push Off (PO), followed by the limb swing (S) [19-20] . HC phase represents the initial contact ground of the limb. It begins with HS event and ends when the foot is completely in contact with the ground. FFC is the phase in which the foot is completely in contact with the ground, the upper body loads the body weight on the leg. It ends when the heel leaves the ground. PO phase represents the stage in which the leg prepares for the swing phase. It begins when the heel starts to rise up from the ground and ends when toe loses contact with the ground (TO event). The transitions events between Heel Contact and Flat foot Contact phase and between the Flat foot Contact and Push Off phase are known as mid-foot strike (MS) and heel rise events (HR), respectively. To the best of our knowledge, the machine-learning-based approach mentioned above [18] has never been tested on the multi-class classification of the four gait-sub-phases. This is expected to lead to a deterioration of classification performances, compared to a simpler binary classification. Thus, the possibility of providing a classification of 4 gait sub-phases by means of a reliable approach is still an open issue.

In the present study, a recurrent neural network (LSTM neural network) approach is proposed for the classification of four gait sub phases of the gait cycle (Heel contact, flat foot contact, push off and swing phase) and the consequent prediction of gait events (Heel Strike, Mid foot strike, heel rise and toe off event), considering only sEMG signals as input to the LSTM model. To this, sEMG signals from Tibialis Anterior, Gastrocnemius Lateralis, Rectus Femoris, Vastus Lateralis, and Hamstring muscles were acquired from both legs of 30 healthy subjects walking barefoot on the floor for about 5 min at their own pace following an eight-shaped path on the ground. Moreover, the aim of study is pursued in condition similar to everyday walking, characterized by a great variability of sEMG signals and spatial/temporal gait parameters due to acceleration, deceleration, reversing, and curves walked during the acquisition procedure [21-24]. This is expected to affect the performance of stride-time prediction compared to straight or treadmill walking but improve the generality of the results.

The thesis is organized in seven macro-chapters: Chapter 2 present a brief review of related works for gait phase classification based only on electromyographic signal (sEMG). Chapter 3 reports an overview of gait analysis and electromyographic signals. In addition, the gait sub-phases classified in this research are defined. Chapter 4 present the various machine learning techniques and in particular, the model implemented in this study. Chapter 5 describes the network set-up, the acquisition of sEMG

signals and signal pre-processing, the gait sub phase classification through a deep learning approach and gait event identification. Chapter 6 present the results of the described method. In chapter 7 all the results are discussed and study in the present research is concluded.

2. Related Works

Human motion classification using sEMG signals is usually performed by means of machine learning approaches [25-27]. Recent studies proposed several methods for gait phase classification based on feature extraction of the electromyographic signal (EMG). In [10] four time-domain features were extracted from sEMG signals, a Hidden Markow Model (HMM) structure was determined corresponding to the division of the gait cycle. The parameters of the model were estimated with Braum-Welch algorithm. In [11] is described some standard feature extraction methods along with Linear Discriminant analysis classification algorithm to separate 8 different phases of the gait cycle by using electromyographic data of the lower limb. The sEMG signals were collected from quadricepes, hamstring, gastrocnemius, and tibialis anterior muscles. The angular data from the hip was used to assign labels to each EMG data. Principally, time-domain features were extracted from sEMG signals: mean absolute value, waveform length, variance, slope sign changes. The classification accuracy was defined as the number of times the test data is classified into their corresponding gait cycle phases correctly. It was reached a mean classification accuracy of 75%. In [28] sEMG data were acquired from vastus medialis, semitendinosus, adductor longus and tensor fasciae latae muscles on subjects performing walking on a treadmill. Five phases of gait were classified using support vector machine (SVM) after EMG de-noising and time-domain feature extraction (integral of absolute value and variance). An average classification accuracy of 93% was reached. In [29] is presented a gait phase classification method based on feature selection over sEMG signals collected from femoral rectus, lateral femoral, medial femoral, femoral two heads muscles and ensemble learning. 20 feature types in time and frequency domain were extracted such as mean, variance, zero crossing, mean frequency, sample entropy and wavelet transform. All sEMG data were collected from three subjects who performed a treadmill walk. Four machine learning algorithms were considered, two of them based on linear discriminator analysis, the other two based on gradient boosting decision tree algorithm. These multiclass classifiers were introduced in gait recognition for discriminating six different gait phases (Pre-Swing, Mid-swing, Terminal-swing, Pre-stance, Mid-stance, and Terminal stance phase) The four learning methods were compared: tree decision algorithm reached an average classification accuracy of 94% on test data. In [30], it was studied a neural network classifier which combined an LSTM neural network with a MLP (multilayer perceptron) neural network to extract sEMG features and classify five gait sub-phases (pre-stance, mid-stance, terminal-stance, and swing phase). The sEMG signals were collected from three subjects who performed a treadmill walk under five different experimental conditions (at different walking speeds). sEMG data extracted from tensor fasciae latae, semitendinosus, adductor longus and vastus

medialis muscles of right leg and plantar pressure signals measured with pressure insoles placed under the toes and heels were used to train the neural network. The overall classification accuracy varied, passing from 94% to 88% in base of the type of experimental condition. All the studies just mentioned above, were based on feature extraction from sEMG signals collected from subjects (up to four) who performed a treadmill walk. In each study, the different sets of features were used as input to the machine learning stage. Furthermore, no article mentions the prediction error in detecting gait events, this means that, even if the accuracy value is high, if the errors are concentrated near the point of transitions, unsatisfactory results will be obtained in terms of time error of gait events. In more recent studies [15] a different approach was introduced: the original sEMG signal was first pre-processed (motion artifact, high frequency noise was removed) to obtain a smoothed signal, the envelope was extracted, and then neural networks were used to learn hidden features to classify the main gait phases (stance and swing phase) and then identify the Toe off and Heel strike event as the transitions between the two phases. The sEMG signals were acquired during level ground walking from tibialis anterior, gastrocnemius lateralis, medial hamstring and vastus lateralis muscles of each leg from 23 healthy adult subjects. The classifier (a multilayer perceptron neural network) was fed with the envelope of sEMG signals. Heel strike and toe off events were predicted with a mean absolute error of 21.6 ± 7.0 ms and 38.1 ± 15.2 ms, respectively and an average accuracy of 99%. The approach described in the present research, represent an evolution of the last one, moving from a binary classification to a multi-class classification using recurrent neural networks. A classification of the main four sub-phases and the prediction of transitions moment between two phases is performed starting from sEMG only.

3. Gait Analysis

The gait cycle (GC) is defined as the time interval between two successive occurrences of one of the repetitive events of walking. It begins in the instant at which one-foot contacts the ground. The floor contact is initiated with the heel defined as heel strike (HS), but not all the people have this capability, so the term Initial Contact is used to designate the onset of the gait cycle [1]. If it is decided to start with the initial contact of the right foot, then the cycle will continue until the right foot contacts the ground again. The left foot goes through the same series of events as the right foot but displaced in time by half a cycle. The main gait-phases of the cycle are Stance and Swing phase. Stance phase (which is also called 'Support phase' or 'Contact phase') is the period in which the foot is in contact with the ground, and it begins with the Heel contact (the onset of the stance phase). Swing phase is the period in which the foot is moving forward through the air, it begins as the foot is lifted from the floor defined as Toe-Off event (TO) [31]. In [31] the gait cycle is divided into eight periods, five of which occur in the stance phase and three in the swing phase as shown in *Figure 3.1*. The stance phase is subdivided in four sub phases: Initial Contact (Heel Contact), Loading Response and Mid-Stance (foot flat contact), Terminal Stance and Pre-swing (push off). The swing phase is divided into three sub-phases: Initial Swing, Mid-Swing, Terminal swing.

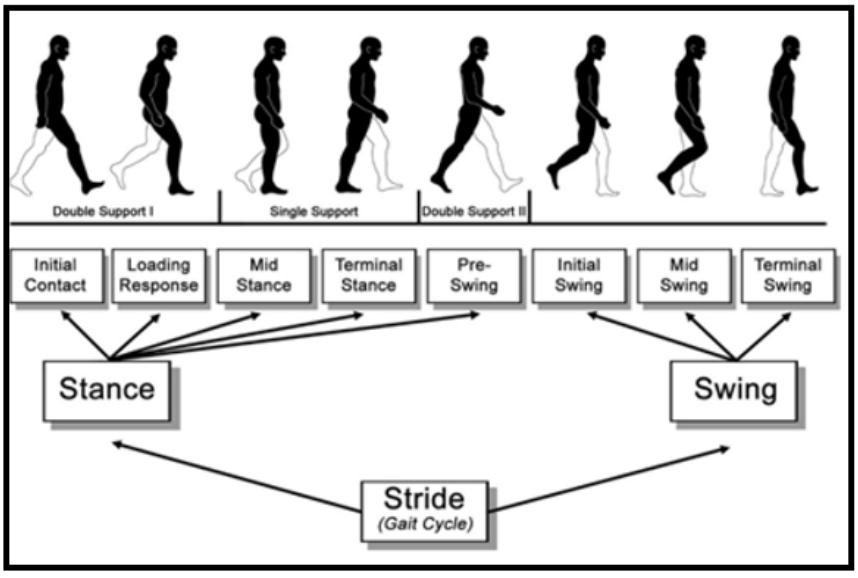

Figure 3.1. Gait cycle subdivision (reference leg the shadow leg). Stance phase (60% GC) and Swing phase (40% GC). At the start and end of stance phase both the feet are in contact with the ground (double support phase). In the middle portion one foot is in contact with the ground (single support phase).

Both the start and the end of stance phase involves a period in which both feet are in contact with the ground (Double support), the body weight is shared equally by both feet. In the middle portion of stance phase only one foot is in contact with the ground (single support phase), the entire's body weight is supported by only one leg. The duration of a complete gait cycle is known as the cycle time (100% GC) which is divided into stance time (60% GC), the average duration of the stance phase is approximately 0.59 to 0.67 s, and swing time (40% GC), this phase lasts, on average, 0.38 to 0.42 s. The average duration of one gait cycle for men ranges from 0.98 to 1.07 s [32]. The initial double-leg support represents the initial 10% of the GC, the single-leg support is the next 40%, and the terminal double-leg support concludes the stance period with another 10% of the GC. However, speed of walking can affect these percentages with respect to the subperiods of stance, where increases in speed will decrease the double-leg support sub-periods and increase single-leg support. Eventually, if we keep moving faster and start running, the double-leg support sub-periods will disappear. On the other hand, decreases in walking speed will have the exact opposite effect [1]. The gait cycle is also defined as stride, its duration is the interval between two consecutive initial contact carried out by the same limb (it is based on the actions of one limb) [33]. Each stride is constituted by two steps. At the midpoint of one stride the other foot contacts the ground to begin its next stance period. *Figure 3.2* shows some terms used to describe the placement of the feet on the ground.

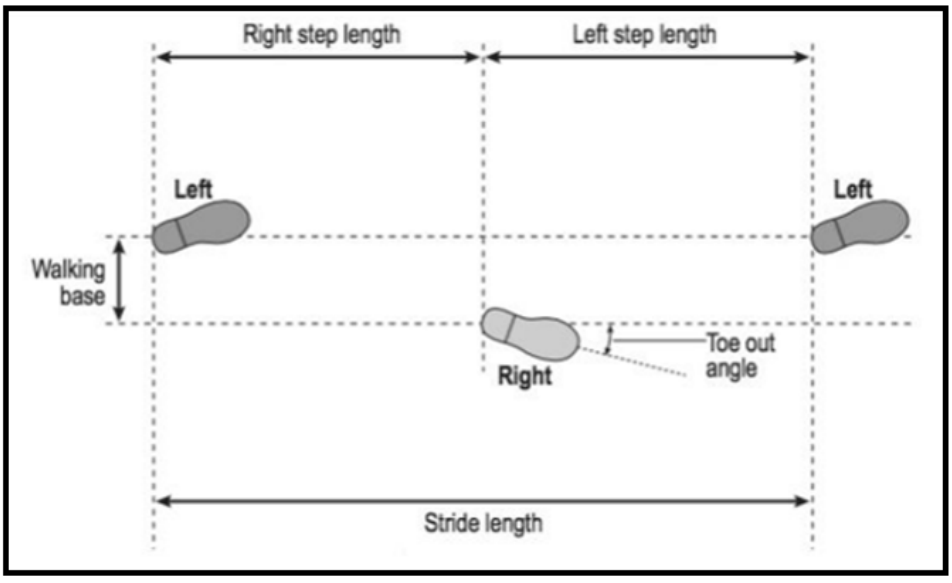

Figure 3.2. Stride length: distance between two successive placement of the same foot and It consists of two steps. The walking base: the side to side distance between the line of the two feet. Toe Out: angle in degree between the direction of progression and a reference line on the sole of the foot.

The sequential combination of the eight phases enables the limb to perform three tasks: weight acceptance (WA), single limb support (SLS), limb advancement (LA). WA begins with the first two gait phases of the stance phase (initial contact and loading response) [31]. The challenge is the transfer of body weight toward to the limb that has just finished swinging forward, it has an unstable alignment.

Initial Contact (0-2% GC): this phase represents the moment in which the foot just touches the floor (HS event). The floor contact is made with the heel. This phase represents the first part of the initial double-leg support period. The stance phase is started with a heel rocker.

Loading Response (0-10% GC): this phase is the rest of the initial double-leg support period. The body weight is transferred towards to the forward limb. It begins with initial floor contact and finishes when the other foot leaves the ground for swing.

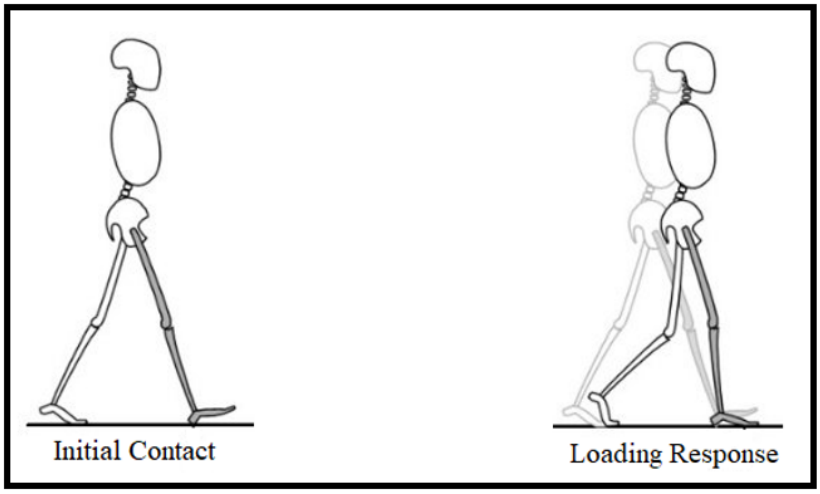

Figure 3.3. Reference limb is the shaded limb. 1. Initial Contact. The ankle is dorsiflexed (neutral position), the knee is extended, and the hip flexed. The ground contact is made with the heel. 2. Loading Response. the ankle plantar flexion limits the heel rocker by forefoot contact with the ground.

SLS continues with the next two gait phases (mid-stance and terminal stance). The other foot is lifted the ground for swing, thus begins the single limb support interval for the stance limb until the opposite limb again contacts the ground. All body weight is supported by only one limb. The two main phases involved in SLS are mid stance and terminal stance phase [31].

Mid-Stance (10-30% GC): this phase begins when the other foot is lifted from the ground and the ipsilateral forefoot strikes the ground, event defined as Mid foot strike (MS), so that this is the first part of the single-leg support period. The body weight is aligned over the forefoot.

Terminal Stance (30-50% GC): this phase begins when the heel rises from the ground, event defined as Heel rise (HR); this phase represents the second part of the single-leg support period. the body weight moves ahead of the forefoot, and it finishes when the other foot contacts the ground again.

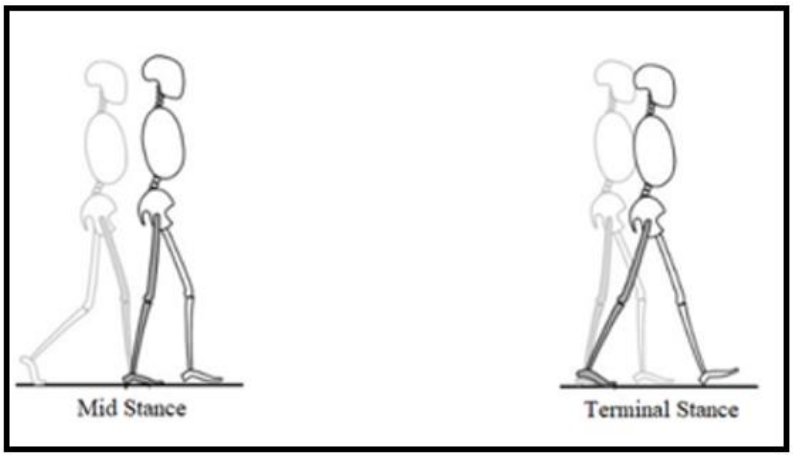

Figure 3.4. 1. Mid Stance. Hip and Knee are extended. The limb advances by ankle dorsiflexion (ankle rocker). 2. Terminal Stance. Knee and hip increase extension. The heel rises and the limb advances over the forefoot rocker.

At this point, the limb is ready to swing, it advances and is prepared for the next stance period. The last sub-phase of stance and three sub-phases of swing are involved in limb advancement [31].

Pre-swing (50-60% GC): this phase represents the terminal double-leg support period. It begins with initial contact of the opposite foot and ends with ipsilateral toe off event.

Initial swing (60-73% GC): this phase begins when the foot leaves the ground (TO event) and ends when the same foot is opposite the stance foot.

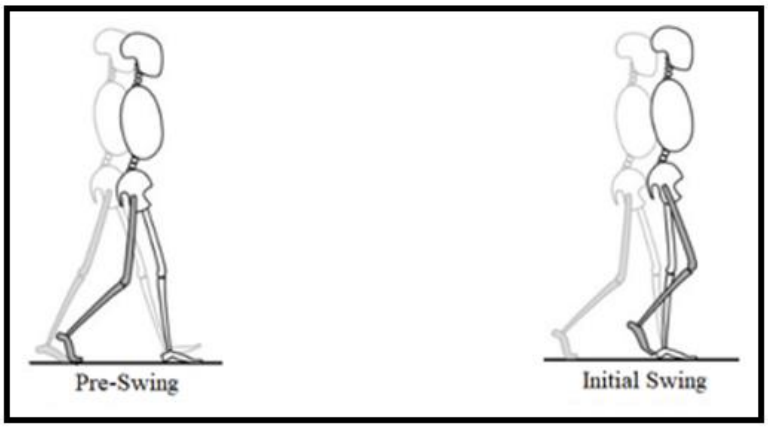

Figure 3.5. Pre-Swing. Ankle plantar flexion increases, greater knee flexion and loss of hip extension. Initial Swing. The foot leaves the ground. Limb advances due to hip flexion and increased knee flexion. The ankle partially dorsiflexes.

Mid-swing (73-87% GC): when the limb is opposite to the stance limb, this phase begins. It ends when the swinging limb is forward with respect to the stance limb and the tibia is vertical.

Terminal Swing (87-100% GC): this phase begins with a vertical tibia and ends before the foot strikes the floor. The limb advancement is complete when the shank moves ahead of the thigh.

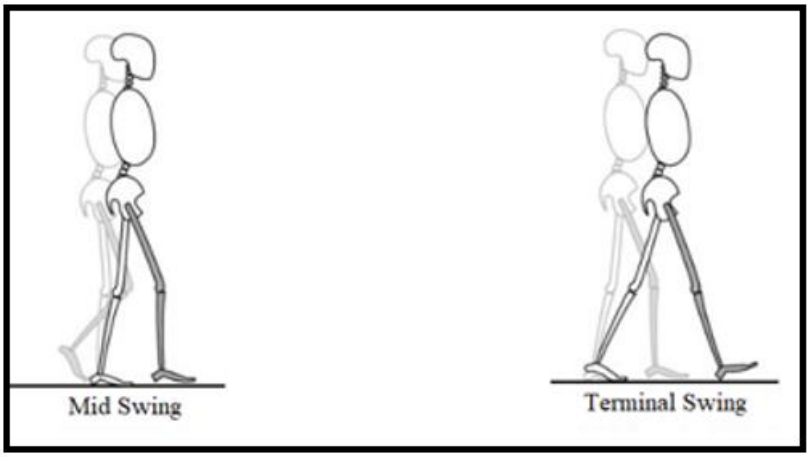

Figure 3.6. Mid Swing. The ankle continues dorsiflexing reaching the neutral position. The knee extends in response to gravity, while the limb advances anterior to the body weight line thanks to hip flexion. Terminal Swing. The ankle reaches the neutral position, the limb advancement is completed thank to knee extension, the hip keeps its earlier flexion.

3.1 Ankle Motion

The ankle joint is related to the junction between the tibia and the talus, also called tibiotalar joint. During the gait cycle, the arcs of ankle motion are not large, it travels through four arcs of motion: it alternately plantar flexes (ankle's downward motion) and then dorsiflexes (upward travel of the foot) [31]. During the swing phase, the ankle only dorsiflexes contributing to the limb advancement. The ankle begins stance phase plantar flexed (3°-5°). With the onset of forefoot contact (foot flat contact) the ankle changes its direction toward dorsiflexion that continues through midstance and first half of terminal stance reaching a peak of 10° by 50% GC. Then, there is an ankle plantar flexion reaching an angle of 30° at the end of the stance phase. The neutral position (around 0°) is reached during mid-swing phase and maintained until the next initial contact phase. The ankle joint motion is controlled by dorsiflexors and plantar flexors muscles [31]. Principally, the plantar flexors muscles are active in stance phase, while the dorsiflexors (pretibial muscles) are swing phase muscle, but there is an exception during the loading response phase of stance, the dorsiflexor muscles participate to control the rate of ankle plantar flexion permitting the foot to be lowered gently to the ground [31]. The ankle range of motion during one gait cycle is reported in *Figure 3.7*.

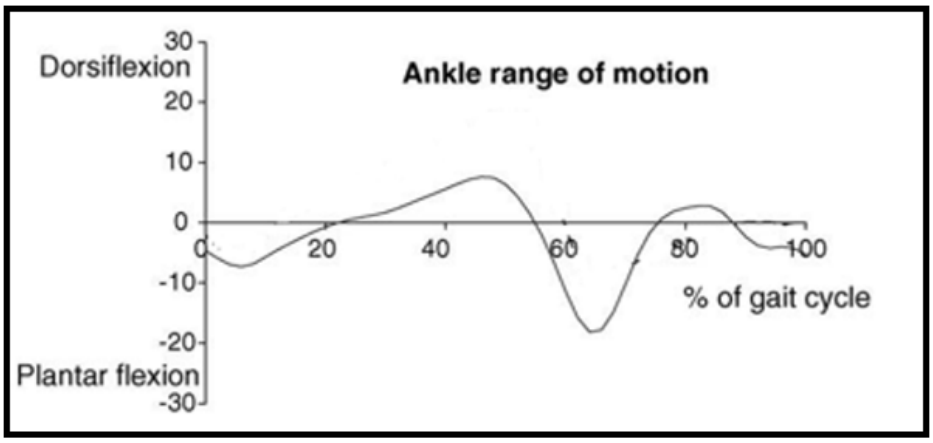

Figure 3.7. Ankle Motion. Adult Normal range during one gait cycle.

Three main muscles lie anterior to the ankle joint: tibialis anterior, extensor digitorum longus and extensor hallucis longus. Their activity starts during the pre-swing phase [31], the first to contract is the extensor hallucis longus then followed by tibialis anterior and extensor digitorum longus contraction during the mid-swing phase. At initial contact all pretibial muscles are active, they terminate their action by the end of the loading response phase. Seven muscles pass posterior to the ankle joint, but soleus and gastrocnemius are the main muscles involved for ankle motion, they form the triceps surae muscle that is the main responsible for plantar flexor motion of the ankle [31]. Near the end of the loading response phase, soleus muscle starts its activity and continues to act throughout mid-stance phase. The contraction of the soleus muscle decreases until to zero by the onset of pre-swing phase. The contraction of gastrocnemius muscle follows the activity of the soleus muscle. It rises in mid stance but is less intense than the activity of the soleus muscle. Then there is a rapid decline and cessation after the onset of pre-swing phase. The loading response presents a high demand on the pretibial muscle group. In this short interval (5% GC), the body weight is dropped onto the heel, so the pretibial muscles are active to decelerate the rate of ankle plantar flexion. During single limb support phase, the first dorsiflexion arc occurs, it is an interval in which gastrocnemius and soleus muscle contract to decelerate the rate of tibial advancement over the foot against the body's progressional forces. During the swing phase, a second dorsiflexion action occur, only the weight of the foot must be controlled by tibialis anterior and toe extensors. *Figure 3.8* shows the main muscles acting on the ankle joint.

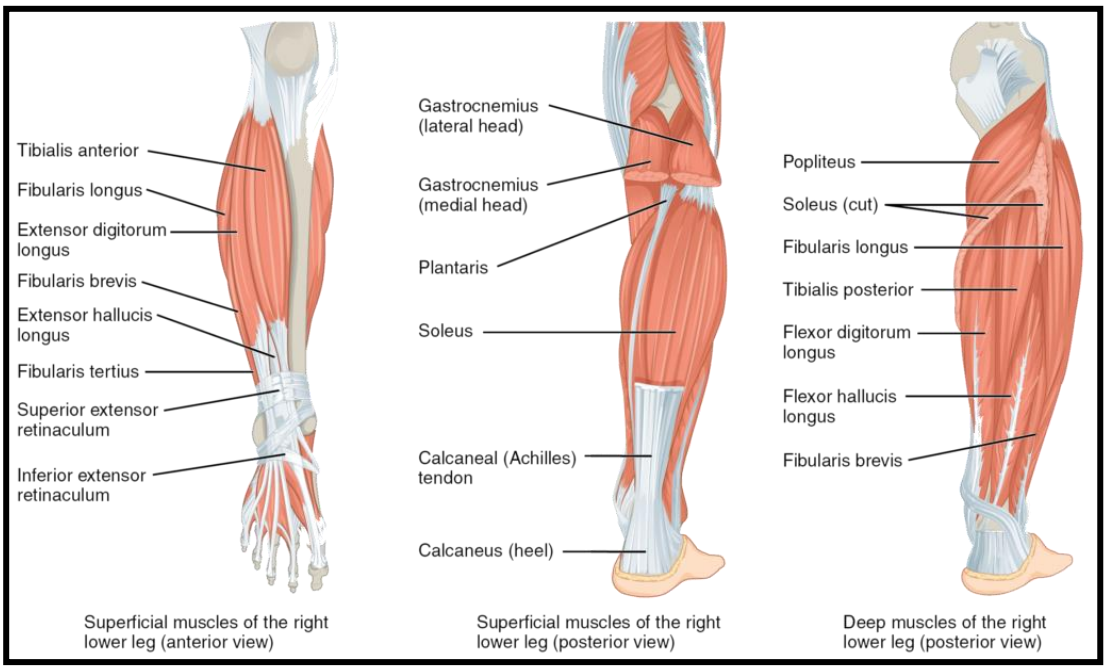

Figure 3.8. Gastrocnemius and Soleus muscle (right lower leg posterior view). Gastrocnemius tendon joins with that of the soleus to form the Achilles tendon which inserts into the back of the calcaneus. Tibialis anterior, extensor digitorum longus and extensor hallucis muscles (right lower leg anterior view). These muscles form the anterior tibial group.

3.2 Knee Motion

The knee is a complex joint characterized by a large range of motion. During stance, the knee is the basic determinant of limb stability, in swing, the knee flexion and extension is the primary factor in the limb's freedom to advance. During the gait cycle, the knee passes through four arcs of motion: it shows two peaks of extension and flexion [31]. At initial contact is flexed about 5° and then flexes throughout the loading phase reaching the peak of flexion with the onset of single limb support (12% GC). During the mid-stance phase, the knee gradually extends. The minimum value of flexion (around 3°) is reached in terminal stance phase (62% GC). Then, with the onset of double limb support the knee flexes again. 40° is reached by end of the pre-swing phase (62% GC). After a pause in mid swing, the knee begins to extend, the extension continues in terminal swing until full extension (around 3° of flexion) is reached. The final knee posture at the end of terminal swing averages 5° of flexion. Fourteen muscles contribute to knee control, they contract at specific intervals within the gait cycle [31]. In swing phase, both flexor and extensor muscles contribute to limb progression. Among the multiple muscles acting on the knee, six muscles don't act at another joint. These muscles are the four vasti heads of the quadriceps that extends the knee and two knee flexors, popliteus, and short head of the biceps femoris. All the other muscles, except the gastrocnemius muscle which has a

primary role as an ankle plantar flexor, also control hip motion (flexion or extension). *Figure 3.9* depicts the knee range of motion during one gait cycle.

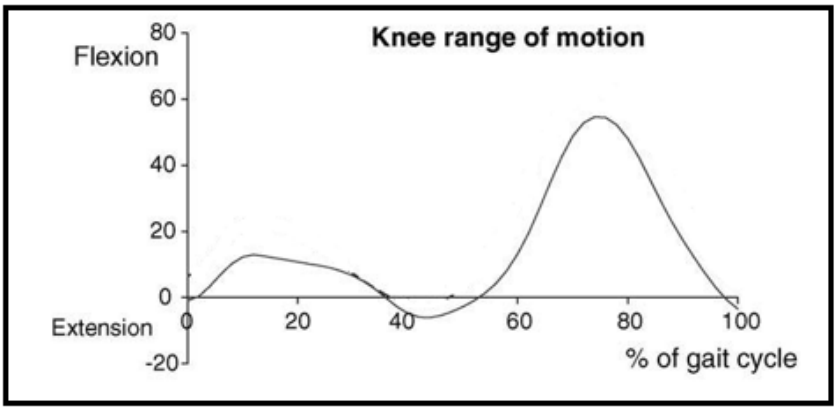

Figure 3.9. Knee Motion. Adult Normal range during one gait cycle.

The quadriceps is the main muscle group at the knee and is the only muscle which extends the knee. Four heads (vastus intermedius, vastus lateralis, vastus medialis oblique and vastus medialis longus) cross only the knee joint (*Figure 3.11*). The fifth head (rectus femoris) includes both the knee and hip [31]. The vasti muscles begins their activity in terminal swing (90% GC) reaching the maximum intensity during the loading response phase. By the 15% of GC, with the onset of mid stance, the quadriceps reduces its effort and ceases. The activity of rectus femoris has a short period of action between late pre-swing (56% GC) and early initial swing (64% GC). Popliteus and the short head of the biceps femoris provide direct knee flexion. The three hamstring muscles (semimembranosis, biceps femoris long head and semitendinosis) are hip extensor but exert a flexor role at the knee (*Figure 1.14*) [31]. In mid and terminal swing until to the first level of loading response phase, these muscles have most intense action. The gastrocnemius muscle is an additional stance phase muscle that principally act at the ankle but is also knee flexor. The gastrocnemius increases its intensity throughout the terminal stance phase (50% GC), then there is a rapid decline of action until it ceases with the onset of pre-swing phase.

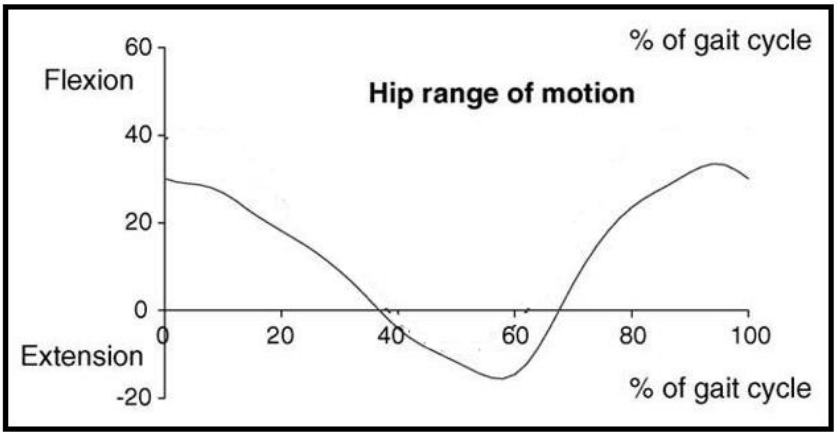

Figure 3.10. Hip Motion. Adult Normal range during one gait cycle.

3.3 Hip Motion

The hip represents the junction between the passenger and locomotor units. During stance, the role of the hip muscles is the stabilization of the trunk, while in swing, the limb control is the primary objective. The hip, during the gait cycle, moves through two arcs of motion: extension during stance and flexion in swing (*Figure 3.10*) [31]. Taking a vertical line as reference line, at initial contact the thigh is flexed 20°. With the onset of mid stance, the hip progressively extends, the thigh reaches neutral alignment at the 38% of GC. During the pre-swing phase the hip reverses its direction of movement and begins flexing. At the end of stance phase (60% GC), the hip reaches a neutral position (0°). Then, the flexion motion continues through the first two phases of gait cycle. The final 25° flexed position of the thigh is maintained within five degrees through terminal swing. During stance phase, extensor and abductors muscles control the hip motion. In stance flexor muscles participate controlling hip motion during limb advancement. The adductors tend to participate during the interval of exchange between swing and stance phase.

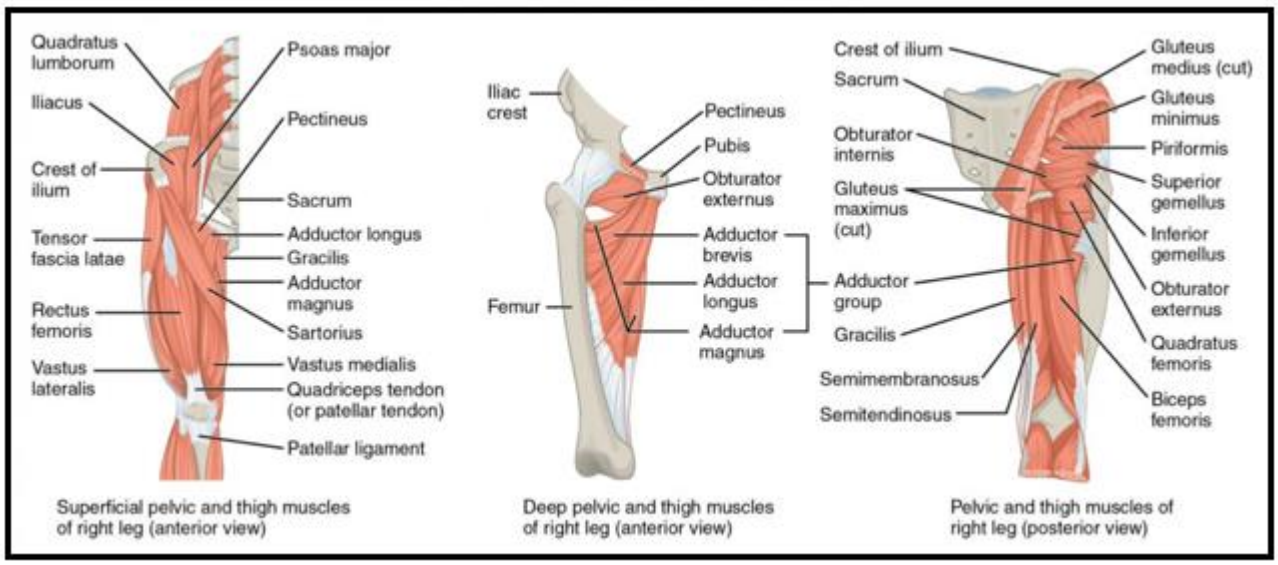

Figure 3.11. Vastus Medialis, vastus intermedius vastus lateralis and rectus femoris are the four elements of the quadriceps muscle (right leg anterior view). Adductor magnus, adductor brevis and adductor longus are the major adductor muscles (right leg anterior view) Semimembranosis, semitendinosis and biceps femoris are the four elements of the hamstring muscles (right leg posterior view).

The hip extensor muscles (hamstring muscles) occur from late and mid swing through the loading response [31]. The hamstring muscles (semimembranosis, semitendinosis and long biceps femoris) start to contract in mid swing (80% GC). The peak effort is reached in terminal swing. Then, all the three hamstring muscles cease their activity during the rest of gait cycle. the adductor magnus begins to contract near the end of terminal swing and progressively the intensity increases throughout the phase. During loading response phase, it remains active and then relaxes. Lower gluteus maximus muscle begins with the end of terminal swing. During loading response phase, it increases its effort level, then rapidly decreases its activity level by the end of loading response phase (10% GC). The abductors are another muscle group functioning during the initial half of stance [31]. Principally, the upper gluteus maximus is the main muscle involved, it begins in terminal swing (95% GC), then the intensity rises during loading response and continues through mid-stance. The flexor muscle action begins in late terminal stance and continues through initial swing and early mid swing. The adductor longus is the first and most important hip flexor, its activity begins in late terminal stance, and it remains active into initial swing. Then, the rectus femoris begins its activity with a brief period of action in pre-swing and early initial swing. High demand for muscular control in stance period is introduced to stabilize the trunk mass, while in swing period, the second demand on the hip musculature to initiate limb advancement is less intense.

In *Figure 3.12* is summarized the typical activity of the major muscles during one gait cycle (0-100% GC). Gluteus maximus, Quadriceps muscles and Triceps surae muscle are principally involved in stance phase, while Iliopsoas, hamstring muscles and tibialis anterior are mainly involved in swing phase.

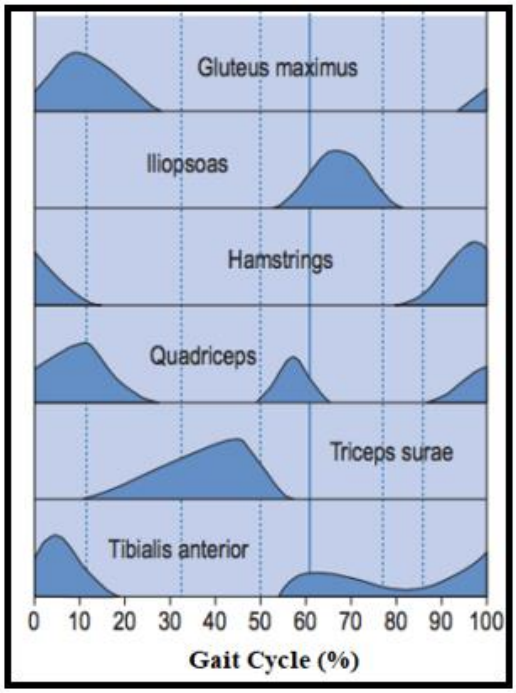

Figure 3.12. Gluteus maximus, iliopsoas, hamstring, quadriceps, triceps surae and tibialis anterior activities during a gait cycle. the blue line identifies the instant (around 60% GC) in which Toe off event occurs. Dashed lines indicate some gait events that occur between two gait phases.

3.4 Gait Cycle Segmentation

In the present study, it has been considered the segmentation of gait cycles following the approach adopted in [19] where each stride is defined as a sequence of the following three sub-phases of stance: Heel Contact (HC), Flat Foot Contact (FFC), Push Off (PO), followed by the limb swing (S). Heel Contact phase (0-10 % GC) begins, by the definition, with the heel strike (HS). Heel strike event represents the initial contact ground of the limb during walking. At HC phase the foot functions are to absorb shock and ensure a stable position. This phase ends when the foot is completely in contact with the ground. The event Mid Foot Strike (MS), where a ground contact of the mid-foot is obtained, indicates the transition moment from the HC phase to the FFC phase. FFC contact phase (10-40 % GC) correspond the period in which the foot assumes more of a support and overall stability role.

During this phase the foot has transformed from a shock absorber and is now in stability role. The body weight is moved forward over the fixed limb and the foot commences a change toward propulsion. The FFC phase ends as the heel begins to leave the ground. The event HR indicates the transition moment from FFC phase to the PO phase. The PO phase (40-60 %) is the final stage of the stance phase. During PO phase the body is propelled forward, and this propulsive moment causes the final TO event where the contact between toes and floor is lost, and the swing phase begins. During the S phase (60-100 % GC) the swinging limb moves in front of the stance limb leading to a forward progression. *Figure 3.13* shows the gait cycle division with the approach just described.

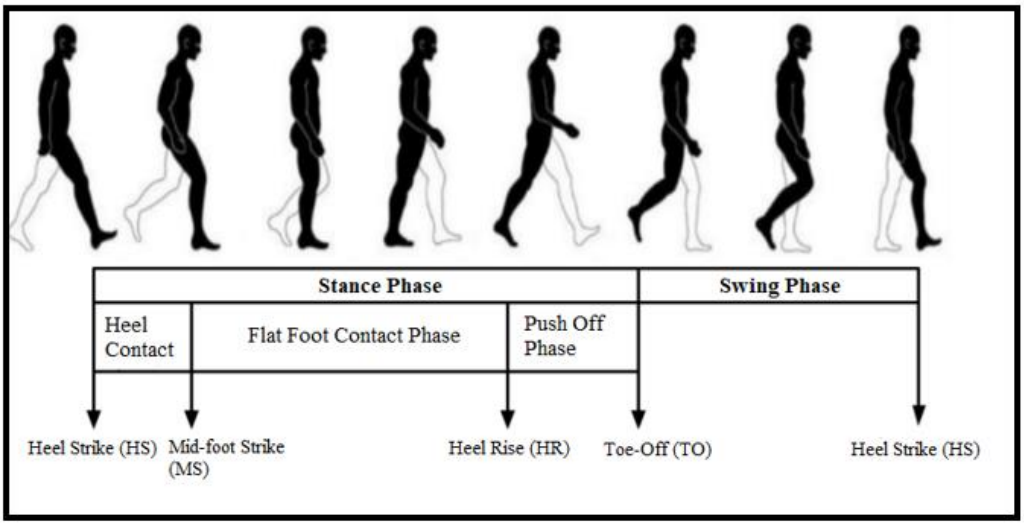

Figure 3.13. Shadow Leg (Reference Leg). Gait Cycle division in Stance and Swing Phase. The stance phase is divided in Heel Contact phase (HC), Flat foot Contact phase (FFC), Push Off phase (PO) and Swing Phase (S). The limits of these phases are defined by four events identified as Heel Strike (HS), Mid foot strike (MS), Heel Rise (HR) and Toe Off (TO).

In the study described in the following chapter, the classification of Heel Contact, Flat Foot Contact, Push Off and Swing Phase and the prediction of the transition moments (HS, MS, HR and TO) between them was performed. In all the studies, the sEMG signals acquired from Tibialis Anterior, Gastrocnemius Lateralis, Rectus Femoris, Vastus Lateralis and Hamstring muscles of both legs were used to feed an artificial neural network. More precisely, the envelopes of the EMG signal were used to train the net. According to the approach described in [20] the footswitch signals were processed in order to identify the different gait cycles and the sub-phases (HC, FFC, PO and S phase). The information derived from the footswitch signals was used as ground truth for the net.

3.5 Overview of the electromyographic Signals (EMGs)

Electromyographic signal is a biomedical signal that measures the electrical activity generated in the muscle due to its contraction representing neuromuscular activity [34]. The muscles exist in three forms: skeletal muscles, cardiac muscles, and smooth muscles. Skeletal and cardiac muscles are classified as striated muscles, characterized by alternating light and dark bands. All three muscle tissues have properties in common: they all exhibit a quality called excitability, as their plasma membranes can change their electrical states sending electrical impulses called action potentials that travel along their membrane [35].

3.5.1 Muscle Contraction

The signal to initiate muscle contraction is an intracellular calcium signal, and movement is created when a motor protein called myosin uses energy from ATP to change its conformation. The skeletal muscle constitutes about the 40% of the total body weight. They position and move the skeleton, attaching to bones by tendons made of collagen. Each muscle is a collection of muscle cells called muscle fibers that, inside each skeletal muscle, such fibres are organized into bundles. Each muscle cell consists of several structures devoted to movements called myofibrils, that represent every single filament into the muscle cells that stretches or contract to generate motion [34]. The arrangement of such filaments, actin, and myosin, provoke the striated appearance of the skeletal muscle fiber. The plasma membrane of muscle fibers is called the sarcolemma, the cytoplasm is referred to as sarcoplasm. Actin and myosin and their regulatory proteins (troponin and tropomyosin) form the sarcomere representing the functional unit of the muscle fiber (a myofibril represent a succession of them) as shown in *Figure 3.14*. The thin filaments are formed by the actin and troponin-tropomyosin complex, while the thick filaments present the myosin structure, so these types of filaments present higher mass with respect to the previous one.

Each sarcomere has the following elements:

- I Bands: contain the actin filaments (only thin filaments).
- A band: contain mainly the myosin filaments, the thick and thin filaments at the outer edges of the A band overlap.
- H zone: Represents the central region of the A band, it is occupied by only myosin filaments.
- M line: it divides the A band in half

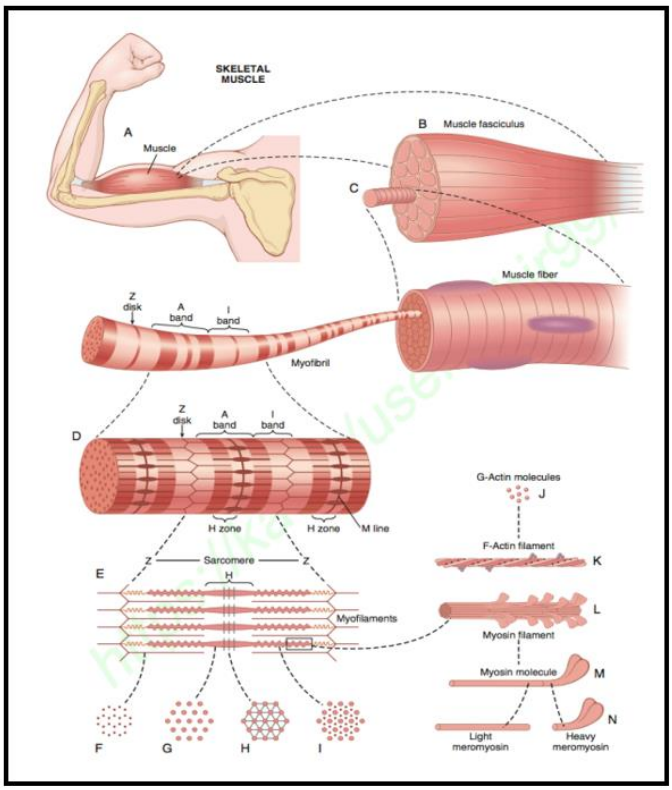

Figure 3.14. Skeletal Muscle, Muscle Fiber, Myofibrils and Sarcomere with the following elements: Z disks, I band, A band.

When the muscle is relaxed, so not signalled by a motor neuron, myosin and actin filaments are not connected, but during contraction with the consumption of energy, actin, and myosin fibers overlap. Actin, myosin are two proteins that constitutes the thin and thick filaments respectively that are involved in the muscle contraction with other two proteins: Tropomyosin and Troponin. When an electrical stimulus is not sent to the muscle, tropomyosin is bind to troponin to form a troponin-tropomyosin complex that prevent the myosin from binding to the actin filaments [34].

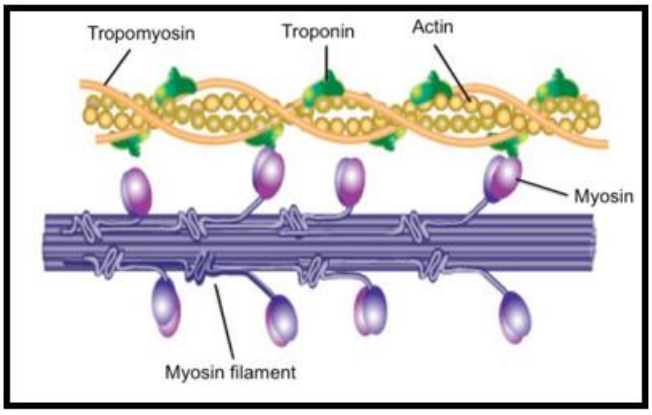

Figure 3.15. Troponin-tropomyosin complex prevent the myosin heads to bind on the actinmicrofilaments.

Before starting the contraction of the fiber muscle, the electrical impulse travels from the efferent neuron (alpha motor neuron) to the muscle fiber by means a neuromuscular junction (synapse formed by the contact between a motor neuron and muscle fiber), then the contraction is a combination of electrical and mechanical events: the action potential reaches the synapse and initiates the action in the muscle fiber thanks to the action of a neurotransmitter (Acetylcholine). Inside the membrane of the muscle fiber, if a certain threshold level exceeds (because of NA+ influx that provoke a depolarization of the membrane) an action potential is caused, changing the membrane potential value from its resting value of -80 mV to 30 mV. The resting action potential is restored by means of a repolarization process and followed by a hyperpolarization period of the membrane (*Figure 3.16*) [35].

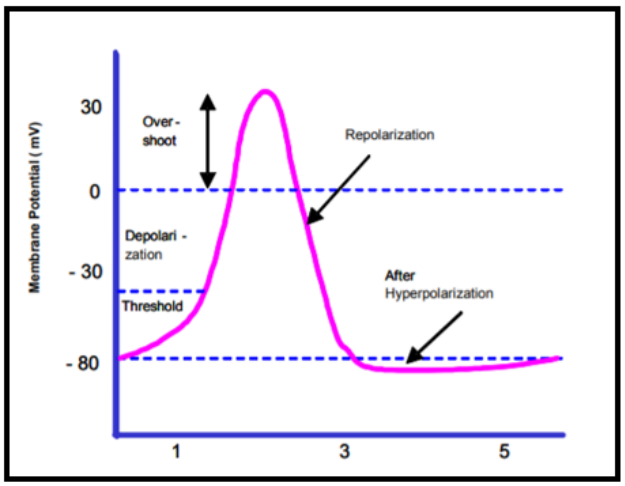

Figure 3.16. Action Potential generated on the muscle fiber membrane. It ranges from a value of -80 mV to 30 mV.

Thus, starting from the motor plate (neuromuscular junction) the muscle action potential spreads along the muscle fiber provoking the calcium release from the sarcoplasmic reticulum that combines with troponin starting the contraction. Infact the shape of the troponin-tropomyosin complex changes leaving free the myosin binding sites, the myosin binds with the actin filaments pulling them towards to the centre line of the H zone provoking a contraction. This process continues until Ca^{++} ions are available. Chemical energy ATP support the process in this way muscle contraction take places [36]. A single motor neuron synapse with a group of muscle fibers, this group together is called motor unit.

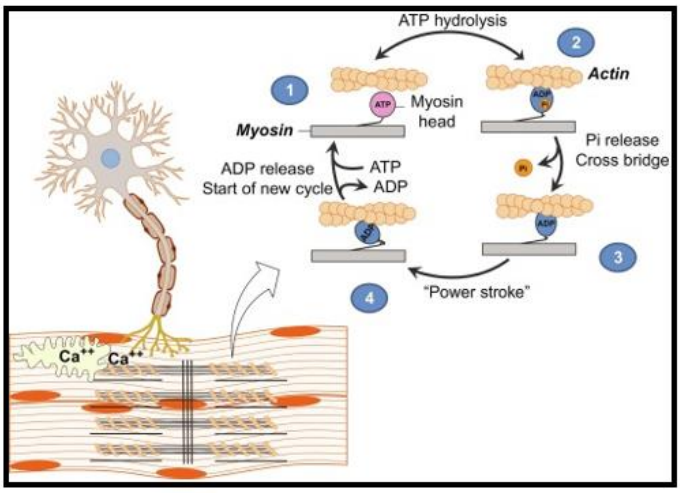

Figure 3.17. Muscle Contraction. Action Potential travels along the muscle fiber provoking the release of Ca^{++}ions that combines with troponin starting the contraction.

3.5.2 Surface EMG Signal

The Emg signal is based on action potentials generated at the muscle fiber membrane resulting from depolarization and repolarization processes. These cycles form an electrical dipole that travels along the surface of the muscle fiber. In general, bipolar electrode configurations, as shown in *Figure 3.18*, are used for EMG measures [37]. In this case, for simplicity, only one action potential traveling on a single muscle fiber is depicted.

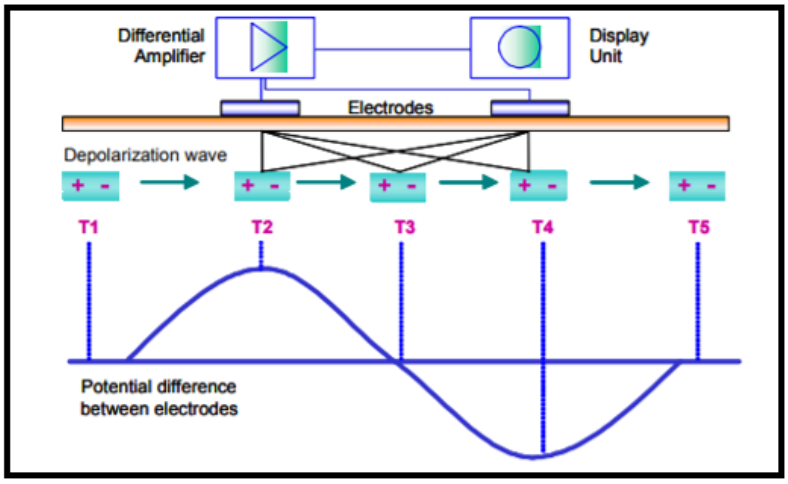

Figure 3.18. Bipolar electrode configuration.

The dipole, depending on the distance between the two electrodes forms a potential difference. Actually, as already said, a motor neuron consists of many muscle fibers, so the electrodes reflect the amplitude of all innervated fibers within the motor neuron. Thus, all the action potentials sum up to, what is called, triphasic Motor Unit Action Potential (MUAP) [38]. The motor unit action potentials of all active motor units detectable under the electrode side are electrically superposed (the resulting signal detected by the electrode is a bipolar signal characterized by positive and negative values). The recruitment (more than one activation of the motor units producing more contraction of the muscle) and the firing frequency (activation frequency of one motor unit) of the MUAP influence the amplitude of the resultant signal (EMG signal).

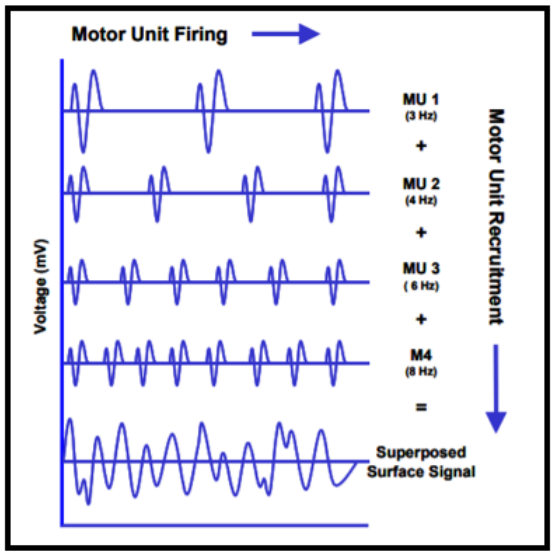

Figure 3.19. All the Motor Unit Action Potential are superposed. The resulting signal is characterized by positive and negative peaks.

The raw Emg signal is the unfiltered and unprocessed signal that detects the superimposed MUAP [37]. The raw sEMG spikes may reproduce the activation of one or more motor units: if they are activated and are near to the electrodes, the signal detected produce a strong superposed spike. Typically, raw sEMG signal range between +/- 5000 mV and have a frequency content between 6-500 Hz. the most frequency power ranges between 20 and 150 Hz. The raw sEMG measured by surface electrodes, are influenced by all the tissues that stands between the electrodes and the source of the signal [37]. sEMG characteristics and shapes can also be influenced by:

- Muscle Cross Talk: it is caused by EMG signals coming from the adjacent muscles. It is possible to eliminate it adjusting the distance between two electrodes (approximately 2 cm) and the electrodes must be placed at the middle of muscle belly.

- External Noise: electrical noise reproduced by external devices.
- Electrodes and Amplifiers: the quality of electrodes and amplifier may interfere the EMG baseline (that must not be higher than 3-5 microvolts).

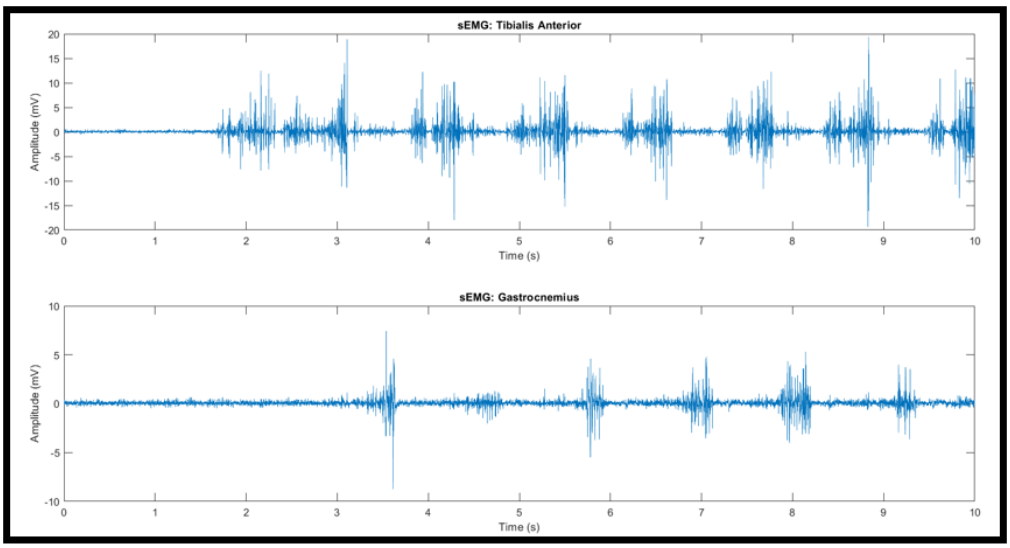

Figure 3.20. Raw sEMG signals of Tibialis Anterior and Gastrocnemius Muscles (T=10s). Sampling Frequency at 2000 Hz. Muscle Cross Talk and Power Line are overlapped on the EMG signal. The Amplitude is given in mV.

The EMG amplifiers act as differential amplifiers to eliminate any type of artifact on EMG signal detected that, due to its sensitive nature, it can be influenced by external noise sources or other type of artefacts [37]. Infact, these amplifiers (built in the cables or positioned on the top of the electrodes), detects the potential difference between electrodes and avoid any other type of interference. Then, the signal is amplified by a factor of at least 500 and a bandpass filter is applied by the amplifier with a frequency range starts from 10 Hz and go up to 500 Hz [39-40]. In *Figure 3.21*, for example, the contribute of Power Noise on sEMG signal is reported. Other main artifacts are:

- Power Noise: it comes from the power line and is transmitted by electrical devices placed near the EMG data acquisition device. (50-60 Hz power line interference).
- DC Offset: Caused by impedance difference between skin and electrodes. It adds an offset value on the raw signal; hence it is not centred to zero.
- Movement Artifacts: artifacts on EMG signal due to the movement of electrodes or cables.
- ECG artifacts: the signal generated by the heart can be picked up by the EMG signal.

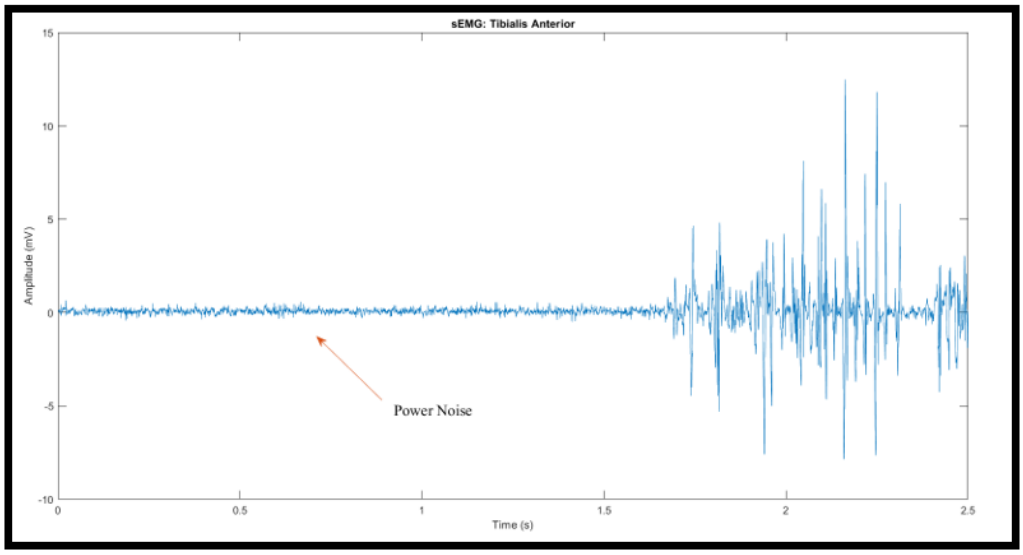

Figure 3.21. Power noise: it comes from the power line. Interference 50 Hz-60Hz.

Before the signal can be analyzed on a computer, an analog and digital conversion is applied with a sampling frequency of at least 1000 Hz in order to preserve sensitive information about the muscles. On the sEMG signals additional digital filters can be applied to remove completely all artifact. The finite impulse response filters (FIR) are filter whose response has a finite duration because it passes to zero in a finite time [41]. For what concern digital FIR filters of order N each value of the output sequence is a weighted sum of the recent input. It is defined by the following equation:

$$y[n] = b_o x[n] + b_1 x[n-1] + \cdots + b_N x[n-N] \qquad 3.1$$

Where:

- $x[n]$: input signal.
- $y[n]$: output signal.
- N: filter order.
- b_i: Value of the impulse response at the i^{th} instant for $0 \leq i \leq N$ of an N^{th} order FIR filter.

An FIR filter is designed by finding the coefficients (b_i) and filter order (N) in base of the specific type of task. Once the sEMG signal is digitally filtered, the linear envelope can be extracted to clarify

the characteristics of the sEMG signal following two-step process [42-44]: Full-wave rectification (negative amplitudes are converted to positive amplitudes, so negative spikes are moved up to positive) and low-pass filter (2^{nd} order low-pass Butterworth filter at a 5 Hz cut-off frequency). The last step that is possible to do is the normalization process. Infact, one drawback of the EMG analysis is that the amplitude of signal strongly depends on a given signal acquisition. Different measures are obtained even if the same muscle site is measured. One solution is to normalize to a reference value, for example, the maximum voluntary contraction (MVC) value (patients reproduce a maximal contraction) [37]. The MVC test is performed for each muscle that is investigated during the experiment. Another normalization process can be done using the peak value of an Emg signal as reference point (applied on filtered rectified EMG signal) and the main effect that is obtained is the reduction of the variability (variance) of the signal [37]. By means of the normalization process all the data are scaled from microvolts values to percent with respect to the reference value. The shape of the EMG curve doesn't change, but Y-axis is scaled.

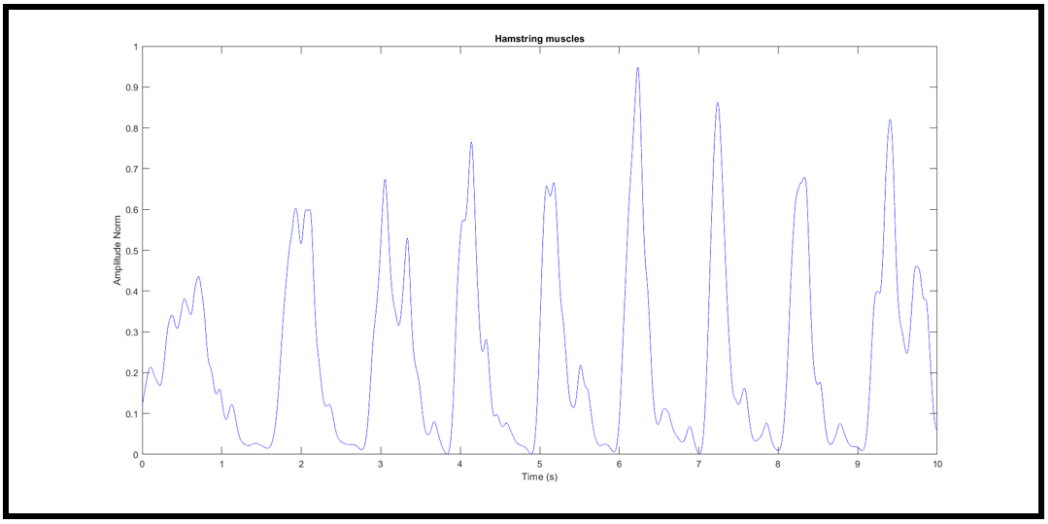

Figure 3.22. sEMG signal acquired from hamstring muscles during level ground walking (T=10s). Low-pass and high pass FIR digital filter (cut-off frequency of 450 Hz and 20 Hz respectively). Full-Wave rectification and Normalization were performed. The peak value of the Emg signal was used as reference for the normalization. The amplitude is expressed as percentage of the reference value.

4. An Overview of Machine and Deep Learning

Artificial intelligence (AI) is a very large research field, where machines show cognitive capabilities, for instance learning behaviours, proactive interaction with the environment, inference and deduction, computer vision, speech recognition, problem solving, knowledge representation, perception. Artificial Intelligence represents any activity in which machines simulates intelligent behaviours shown by humans [45]. It takes inspiration from elements of computer science, mathematics, and statistics. The Machine learning (ML) is a subbranch of AI that focuses on teaching computers how to learn without the need to be programmed for specific tasks. The idea behind machine learning is that it is possible to create algorithms that learn from data and then is able to make predictions [45]. There are three wide categories of Machine Learning:

- Supervised Learning: In supervised training, both the inputs and the outputs are provided. The network then processes the inputs and compares its resulting outputs against the desired outputs. Errors are then propagated back through the system, causing the system to adjust the weights which control the network. This process occurs over and over as the weights are continually updated. The set of data which enables the training is called the training set, which is used to fit the parameters (weight connections). During the training of a network the same set of data are processed many times in order to optimize connection weights. The set of data in which the model is used to predict the responses is the validation set that provides an evaluation of the model fit. Finally, the test data set is a data set used to provide an unbiased evaluation of a final model fit on the training data set.
- Unsupervised Learning: input data are given to the machine; it has to find the best structure by itself with no external supervision.

Deep learning (DL) is a particular subset of Machine Learning methodologies using artificial neural networks (ANN) slightly inspired by the structure of neurons located in the human brain [45]. The word “deep” refers to the presence of many layers in the artificial neural network, a network is considered as deep when it has hundreds of layers. In a Deep Learning artificial neural network, the hidden layers have the function of learning features of the input data that best fit the task at hand. This makes so that inputs of a Deep Learning model are often raw data, without the need for features engineering, which is performed internally by the neural network [45].

4.1 Neural Network

Artificial neural networks (briefly, nets) represent a class of machine learning models, loosely inspired by studies about the central nervous systems of mammals. Each net is made up of several interconnected neurons, organized in layers, which exchange messages (they fire) when certain conditions happen [46]. The network takes inspiration from the human brain. The brain is a collection of about 10 billion interconnected neurons. The neurons are uniquely shaped cells with long processes that extends outward from the nerve cell body into the cell's processes, that are usually classified as either dendrites, which receive the incoming signals, or axons, which carry outgoing information (*Figure 4.1*) [47]. Thus, by means of dendrites and axons, neurons can communicate with other cells or between their selves, forming networks. The region where an axon terminal meets its target cell is called a synapse. A neuron's dendritic tree is connected to a thousand neighbouring neurons. When one of those neurons fire, a positive or negative charge is received by one of the dendrites. The strengths of all the received charges are added together through the processes of spatial and temporal summation.

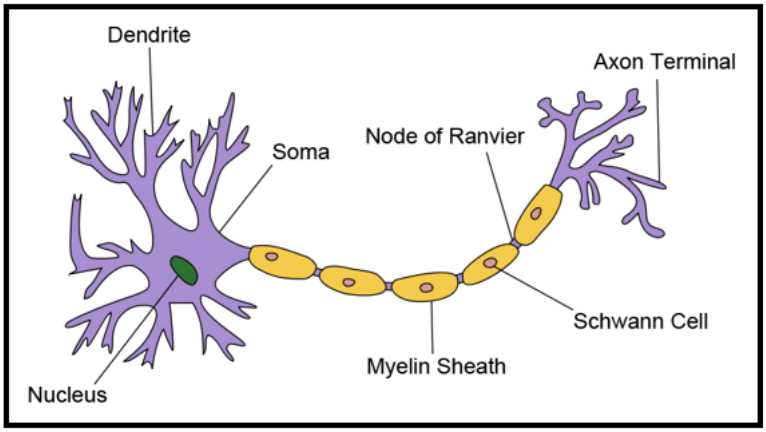

Figure 4.1. Biological Neuron. Each neuron is a cell that uses biochemical reactions to receive, process and transmit information.

In the neural network, neurons are arranged in layers, each neuron is a simple processing unit which takes one or more input and produces an output. At each neuron, every input has an associated weight which modifies the strength of each input. The neuron simply adds together all the inputs and calculates an output to be passed on as shown in *Figure 4.2*. The neuron structure can be split in two parts: in the first part weights associated to input values and bias are summed, the second part computes the neuron's output by means of the activation function [45].

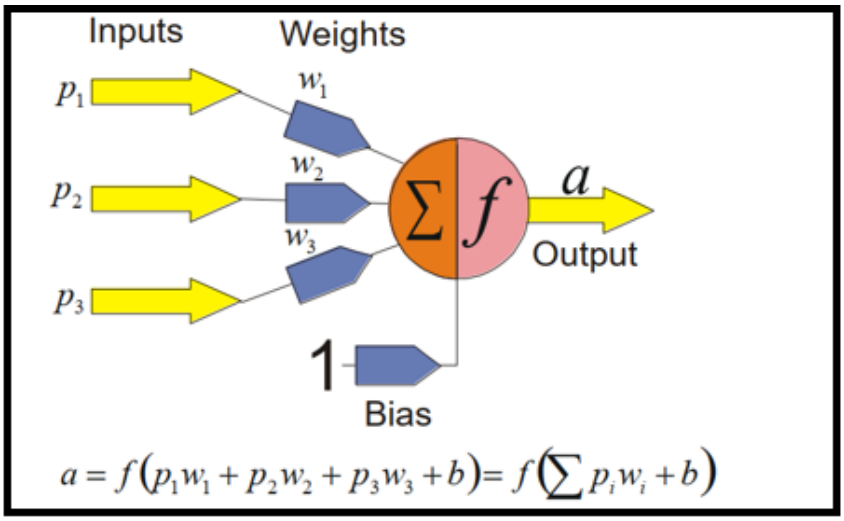

Figure 4.2. Neuron structure. The output of the neuron is given by the output of the activation function that takes as input weight associated to the input and a bias value associated to the neuron.

The perceptron is a simple function which, given an input vector x of m values ($p1, p2.$ ..., p_n) often called input features or simply features, outputs either 1 (yes) or 0 (no) [45]. Mathematically, the function is defined as:

$$f(x) = \begin{cases} 1 & wx + b > 0 \\ 0 & otherwise \end{cases} \qquad 4.1$$

Where w represents the weight and b the bias. According to the values assigned to w and b, the hyperplane defined as $p_iw_i + b$ changes its position. The output of the algorithm can be 1 (yes) or 0 (no). The training process occurs in order to define the values of w and b. Ideally, a set of training data are provided to the network, in this way the computer adjusts the weight and bias in such a way the errors produced in the output are minimized. Unfortunately, the perceptron does not show this little-by-little behaviour, this means that between 0 and 1 there is a big jump. Thus, exist smooth functions that are function that progressively changes from 0 to 1 with no discontinuity (continuous functions).

4.2 Multilayer Perceptron Neural Network

The model with a single linear layer was given the name of perceptron. A model that has multiple layers is called multilayer perceptron neural network [45]. In the *Figure 4.3* is represented a generic neural network with one input layer, one hidden layer and one output layer.

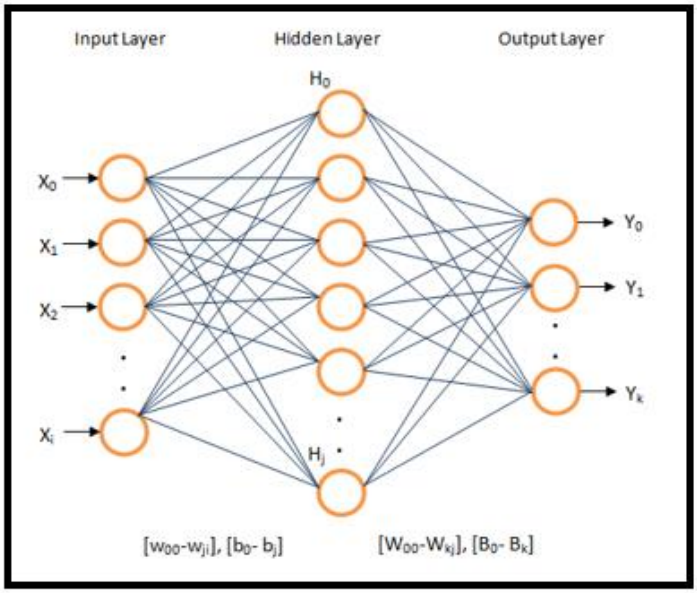

Figure 4.3. Generic Structure of a multilayer perceptron neural network. X represents the input vector; Y represents the output vector (Predictions of the network).

In the diagram, we can observe that each node in the first layer receives an input and fires according to the predefined local decision boundaries. Then, the output of the first layer is passed to the second layer, the results of which are passed to the final output layer consisting of more than one neurons. The net is dense, meaning that each neuron in a layer is connected to all neurons located in the previous layer and to all the neurons in the following layers. The activation function is used to map the resulting values in a range between 0 to 1 or -1 to 1, depending on the activation function: Sigmoid, ReLU, or Tanh. This allows to then choose a threshold (0.5 or 0 as default values) to distinguish false from positive results [45].

The Sigmoid function overcomes the limits presented by the perceptron algorithm. It is defined as:

$$\sigma(x) = \frac{1}{1 + e^{-x}} \qquad 4.2$$

The input varies between negative values and positive values, it produces small output changes between 0 and 1. So, mathematically this function is continuous. The sigmoid function can be used to produce nonlinear output. A neuron with sigmoid function, as activation function, has a behaviour similar to the perceptron algorithm, but the changes are gradual [45]. In *Figure 4.4* is reported an example of sigmoid function.

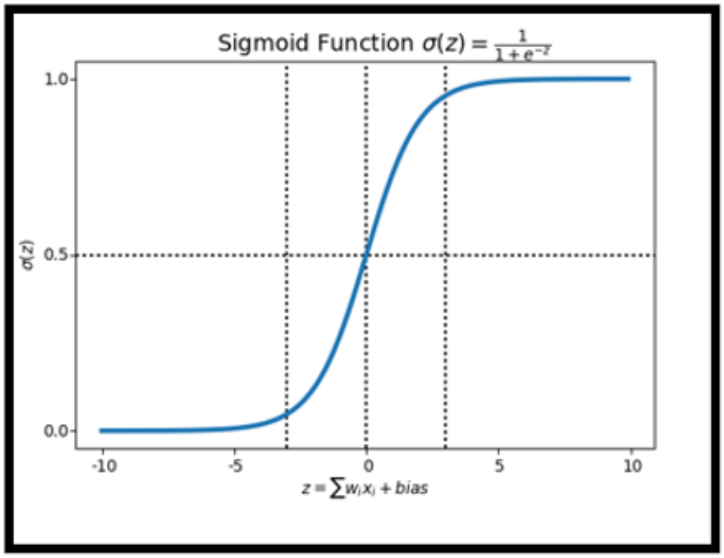

Figure 4.4. Sigmoid Function. Y axis function's output (0-1). X axis input vector z (sum of the products between weight (w_i) and input (x_i) and the bias value).

The sigmoid function is not the unique smooth function present in the neural networks. The Rectified Linear Unit function (ReLU) is defined as:

$$f(x) = \max(0, x) \qquad 4.3$$

The function is 0 for negative values and it grows linearly for positive values.

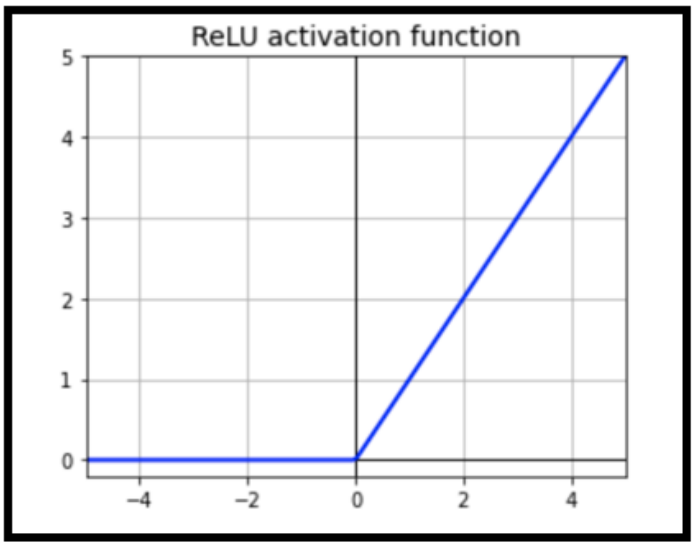

Figure 4.5. ReLU activation function. The output values are different from zero for positive values of the input vector.

Tanh activation function is similar to the sigmoid function (s-shaped), but the range of tanh function is between [-1 1].

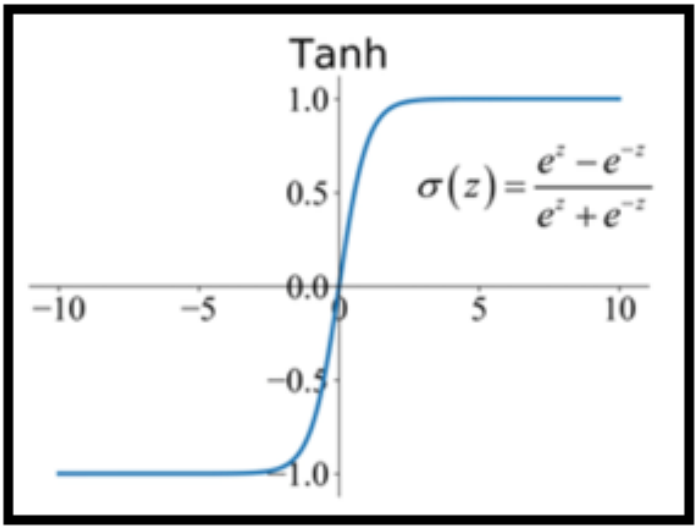

Figure 4.6. Tanh activation function. It ranges between -1 and 1.

The multilayer perceptrons neural network learn from training data by means a process called backpropagation [45]. Each neural network layer is characterized by a set of weights that determines, for a set of input data, the output values. The process of backpropagation means that mistakes are progressively correct once they are detected. At the beginning all the weights have a random assignment. Each value of input in the training set is propagated forward from the input stage, the neurons process the input data giving in output the resultant values that travel layer by layer until the

result reach the output layer where the prediction is made. The ground truth (the actual value) for each input value is known, it is compared with the estimated output and the error made in prediction can be measured (error value). Then, the working key of the backpropagation process is to propagate the error back, from the output layer to the input layer trough the hidden layers, an appropriate optimization function is used to update the weights in the network with the goal of reducing the error value. Tuning the weights has the effect of teaching the network. The network learns. This process is repeated several times until the error is minimized (below a certain threshold value).

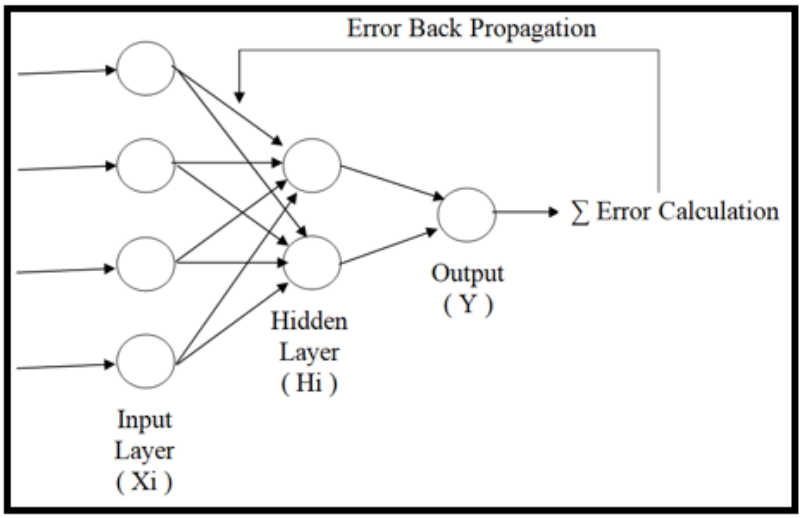

Figure 4.7. Error Back Propagation using a specific optimization algorithm. The neural network weights are adjusted to reduce the error value.

4.3 Recurrent Neural Network (RNN)

The Recurrent Neural Network (RNN) are a class of neural network that exploits the sequential nature of their input [45]. Considering the traditional multilayer perceptron neural network in which all the inputs are considered independent of each other, in a RNN the assumption is that they are arranged in a sequence (e.g., temporal). For instance, inputs could be time series values where the occurrence of one element in the series depend on the elements that appeared before it, exhibit a dependence on past data. The overall RNN can be thought as a net of RNN cells and, for each element of the sequence, the RNN cell performs the same operation. Each cell has a hidden state (memory slot) that considers the dependencies of the present data with the past data that RNN cell has already seen. The value of this hidden state at the instant of time t depends on the value of the hidden state at the

previous time instant and the value of the current input at the time instant t as shown in the equation below:

$$h_t = \varphi(h_{t-1}, x_t) \qquad 4.4$$

Where $h_{t-1}$is defined as h_{t-2} multiplied by x_{t-1}, thus the hidden state considers all past input values until to the beginning of the sequence. The RNN incorporates information from long sequences. A simple representation of the recurrent neural network is shown in *Figure 4.8*:

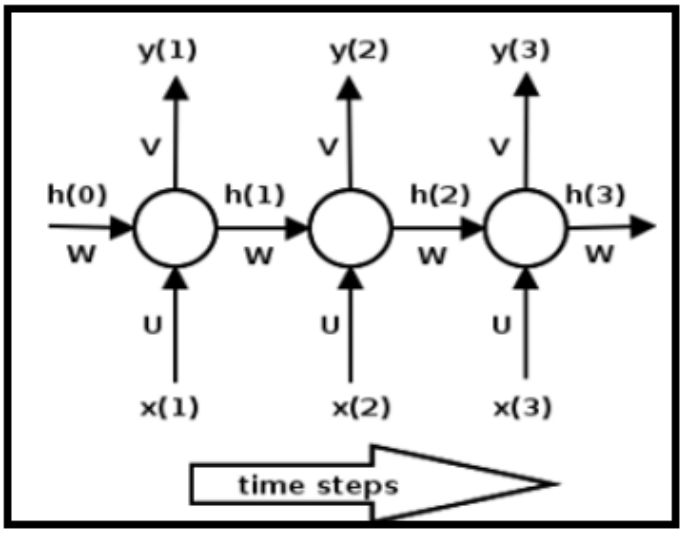

Figure 4.8. RNN's cell. U, V, W are the weight matrices.

Considering the instant of time t_1, the cell takes as in input x_1 and produces the output y_1. The internal state of the cell at the time 1 is given by the sum of the product of the hidden state at the previous time instant (h_0) multiplied by the wight matrix W and the product between the wight matrix U and the input x_1, the activation function tanh is applied to the result. Then, the output vector y_1 is the product between the weight matrix V and the hidden state at the time instant 1. A sigmoid function is applied to that product. These recurrent equations are applied for all data at each time instant.

$$h_t = \tanh\left(Wh_{t-1} + Ux_t\right)$$
$$y_t = sigmoid(Vh_t) \qquad 4.5$$

4.4 Long Short-Term Memory Neural Network (LSTM)

Long-short term memory network (LSTM neural network) is the best popular recurrent neural structure in deep learning field. LSTM neural network learns which information from the series to remember and which not, by means of three gated units: forget gate, input, and output gates through which the memory of past states can be efficiently controlled [48]. LSTM neural network is used in many areas, mostly in machine learning application field, including speech recognition, natural language processing and other pattern recognition applications [49]. The LSTM neural network can learn long term dependencies. The LSTM networks, instead of considering a single tanh layer to implement recurrence and update the hidden state of the cell, it uses four layers (tanh and sigmoid layers) [45]. The cell remembers values over arbitrary time intervals and the three gates regulate the flow of information into and out of the cell. LSTM networks are well-suited to classifying, processing, and making predictions based on time series data, since there can be lags of unknown duration between important events in a time series [48]. In *Figure 4.9* is shown how the hidden state of the cell is updated from the previous state.

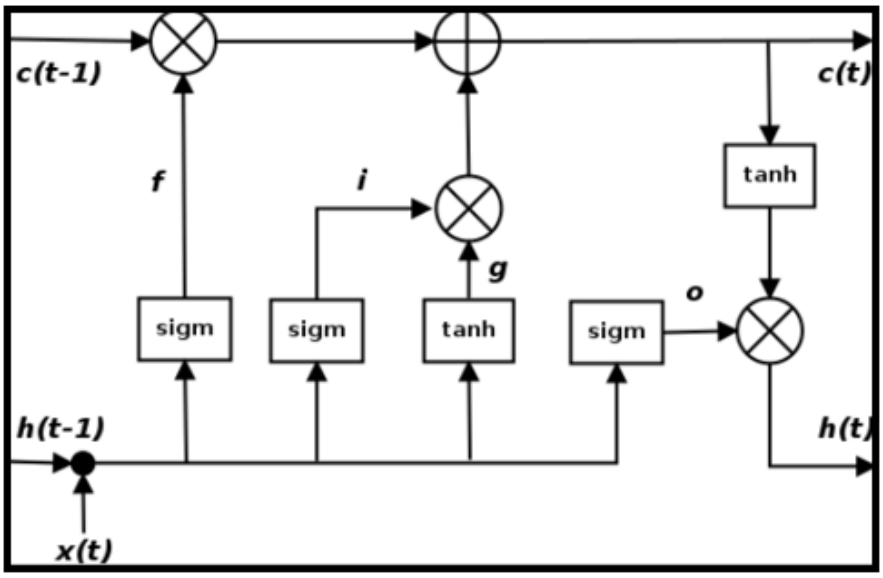

Figure 4.9. LSTM layer uses tanh layer and the other three layers to update the hidden state.

Sigmoid and tanh layers are used to implement recurrence [45]. It is possible to identify the main parameters involved in the updating phase of the hidden state: c(t) (line on the top of the diagram) represents the internal memory of the processing unit. h(t) (bottom line) represents the internal state, i (input gate), f (forget gate), o (output gate) and g are gates, mechanisms by which the LSTM work.

During the learning process the gates values modulate the LSTM's hidden state. The following equations are applied to compute the hidden state at the time instant t [45].

$$i = \sigma(W_i h_{t-1} + U_i x_t)$$

$$f = \sigma(W_f h_{t-1} + U_f x_t$$

$$o = \sigma(W_o h_{t-1} + U_g x_t) \quad 4.6$$

$$g = \tanh\left(W_g h_{t-1} + U_g x_t\right)$$

$$c_t = (c_{t-1} X\, f) + (g\, X\, i)$$

$$h_t = \tanh(c_t)\, X\, o$$

Where:

i: defines how much the current input (x_t) will influence the current computed state.

f: defines if the previous state h (t-1) is allowed to pass through the layer.

o: defines how much of the hidden state h (t) you want to pass to the next layer.

Given i, f, o and g, it is possible to calculate the internal memory of the unit c_t at the time instant t that depends on the previous value of internal memory computed in the previous time instant and the gait values. if i gate is set to zero, the memory is not updated, while setting to 0 f gate, the old memory is ignored. Finally, the hidden state h_t is computed, it is given by the product between the internal memory at the time instant t and the output gate o. A tanh optimization function is applied.

5. Materials and Methods

In the study described in the following chapter, we tried to classify gait sub-phases and predict gait events (transition moments between two gait phases) from sEMG signals. In all the studies, the sEMG signals collected from Tibialis Anterior, Gastrocnemius Lateralis, Rectus Femoris, Vastus Lateralis and Hamstring muscles of both legs were used to feed an artificial neural network (LSTM neural network). More precisely, the envelopes of the sEMG signal were used to train the net. An LSTM neural network was used to classify the main gait sub-phases: Heel Contact (Class 1), Flat Foot Contact (Class 0), Push Off (Class 2) and Swing phase (Class 3). Once the classification is computed, according to the physiological constraints of the gait cycle, the predicted signal was cleaned removing those phases that were too short. On the cleaned signal, gait events between two gait sub-phases were detected: the transition moment between Swing and Heel contact phase (Heel Strike event), the transition instant between from Heel contact and Flat Foot Contact phase (Mid-Foot Strike event), the transition instant between Flat Foot Contact to Push Off phase (Heel Rise event) and the transition moment between Push Off and Swing Phase (Toe Off event). Thus, heel strike (HS) event was identified as the sample in which the transition between the class 3 and 1 occurred, Mid-Foot Strike (MS) the transition sample between class 1 and 0, Heel Rise (HS) the transition sample between class 0 and 2, finally Toe Off (TO) was identified as the sample in which the transition between class 2 and 3 occurred. Finally, to evaluate the performance in predicting the basographic signal, standard classification metrics were used (Precision, Recall, F1-Score) and the mean average error (MAE) defined as the time difference between the predicted event with respect the same event in the reference signal was computed in order to analyze the time transition error between two gait sub-phases. An additional study was done and provided a classification of the two main phases of the gait cycles: Stance (Class 0) and Swing phase (Class 1) and the prediction of the floor foot contact signal (HS and TO events) from only sEMG signals during level ground walking. sEMG envelopes were used to train the net. Then, on the net output, TO event was detected identifying the sample in which the transition between Stance and Swing occurred, HS event was identified as the sample in which the transition between Swing and Stance occurred. This last approach has been already faced in literature [14,15,18,50,51]. Results in predicting HS and TO events provided by this additional study were compared with the ones achieved in literature [14,15,18] to test the reliability of prediction. The studies just described were performed using the open-source web application Jupyter Notebook that uses Python as the programming language.

5.1 Dataset and Signal Acquisition

The dataset included foot-floor contact and sEMG signals recorded during walking on a sample of 30 healthy subjects (16 female, 14 male). These data have been acquired in the Analysis Laboratory of Movement of the University of Politecnica of Marche, Ancona. Subject's characteristics reported as mean value ± standard deviation (SD) was height = 174 ±9 cm; mass = 64.1 ±11.2 kg; age = 23.6±1.7 years. Subjects with a disorder of the nervous system or with a history of orthopaedic surgery were not considered in the study since could affect the performance of walking.

The multichannel recording system, Step 32 (Medical Technology, Italy, Version PCI-32 ch2.0.1. DV, resolution: 12 bit; sampling rate: 2000 Hz) was used to acquire surface electromyographic (sEMG) and basographic signals (signals detected from footswitches). The basographic sensor consists of a rectangular membrane switch, with a side of 11 mm, placed at the end of a strip of flexible plastic material and insulating. At the opposite end, a connector is applied, necessary for connection to the preamplifier / decoder. The basographic sensor make it possible to collect the data relative to the foot-floor contact phase. The footswitches are placed in 3 independent zones: heel (T), first (M) and fifth (L) metatarsal heads and are connected through a wire to a computer. Each lower limb was instrumented with three footswitches under the foot and five sEMG probes, as shown in *Figure 5.1*. The footswitches were activated by a force of 3 N [15].

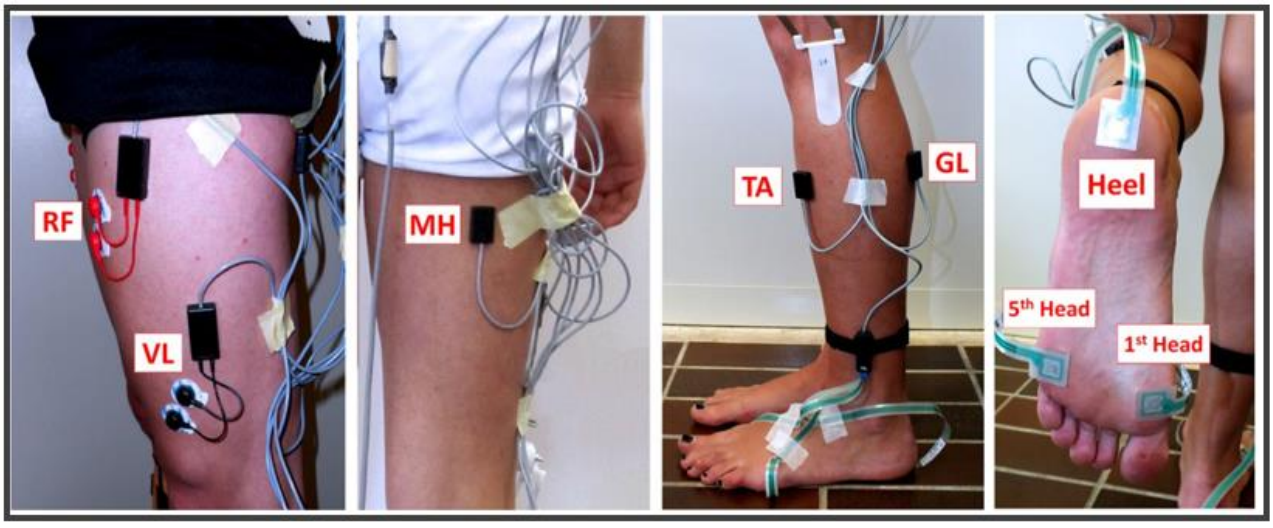

Figure 5.1. Five sEMG signals from each leg were acquired. Rectus Femoris (RF), Vastus Lateralis (VL), Hamstrings (HM), Tibialis Anterior (TA), Gastrocnemius Lateralis (GL) muscles. The footswitches are placed under the Heel, first and fifth metatarsal head.

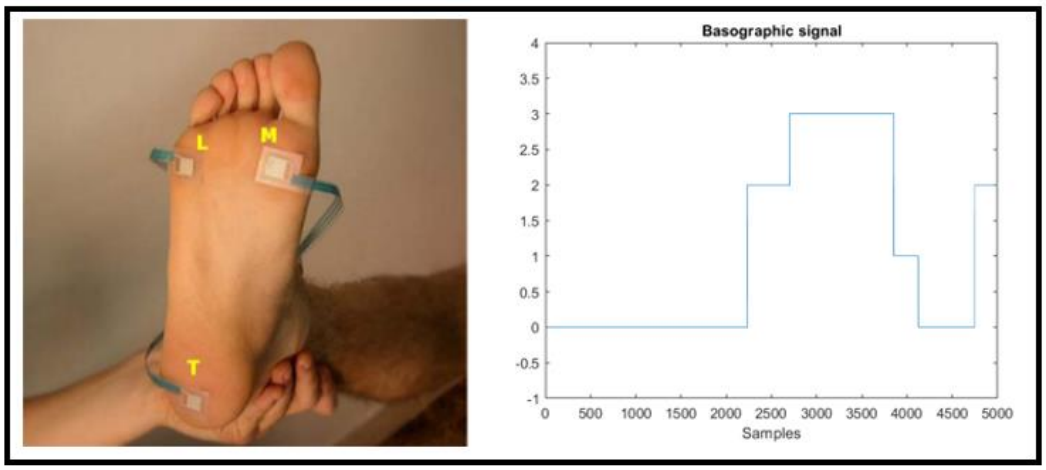

Figure 5.2. 8 gait phases reduced in 4 gait phases. 0 = Flat Foot Contact (FFC), 1 = Heel Contact (HC), 2 = Push Off (PO), 3 = Swing Phase (S).

All the subjects walked following a specific path, information from the footswitches was gradually collected [20]: the Heel Contact phase (HC) occurred when only the footswitch under the heel was closed. The Flat Foot Contact phase (FFC) occurred when the heel footswitch was closed, and at least one of the footswitches under the forefoot was also closed. The Push-Off phase (PO) occurred when the footswitch under the heel is open, and at least one of the footswitches under the forefoot was closed. The Swing phase (S) occurred when all the footswitches were open. Then, gait events were defined as the transition instants between two gait phases: Heel Strike (HS) between S and HC, Midfoot strike (MS) between HC and FFC phase, Heel Rise (HR) between FFC and PO phase, Toe Off (TO) between PO and Swing phase. The *Figure 5.3* schematizes the four on/off combinations of the footswitches and the corresponding gait phases.

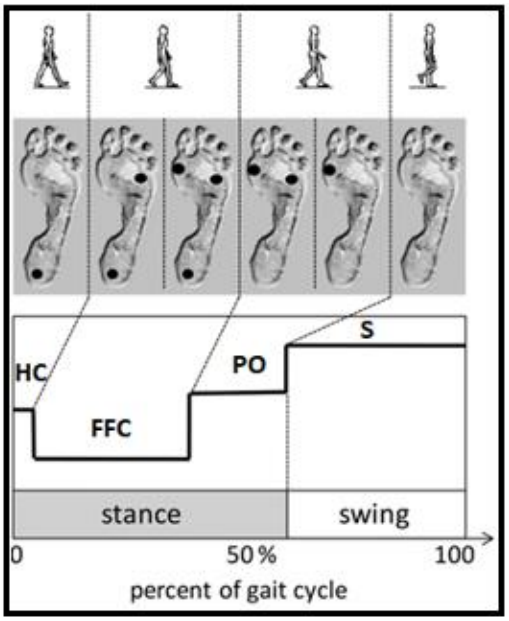

Figure 5.3. Gait phases for one leg: Heel Contact (HC), Flat Foot Contact (FFC), Push Off phase (PO), Swing Phase (S). HC, FFC and PO belong to Stance Phase (60 % of gait cycle).

sEMG signals collected from tibialis anterior (TA), gastrocnemius lateralis (GL) and medial hamstring (MH), were registered by means of three single-differential probes with fixed geometry: (Ag/Ag-Cl disk; electrode diameter: 0.4 cm; gain: 1000; high-pass filter: 10 Hz; input impedance: 1.5 G; CMRR > 126 dB; input referred noise: 1 Vrms) two electrodes are linked to the probe and are at a fixed distance of 8 mm. Furthermore, sEMG signals collected from vastus lateralis (VL) and rectus femoris (RF) were registered by means of two single-differential probes with variable geometry: (Ag/Ag-Cl disks; gain: 1000, high-pass filter: 10 Hz, input impedance >1.5 G, CMRR >126 dB, input referred noise 200 nVrms) two electrodes are positioned at a variable distance on the patient, starting from a minimum of 12 mm.

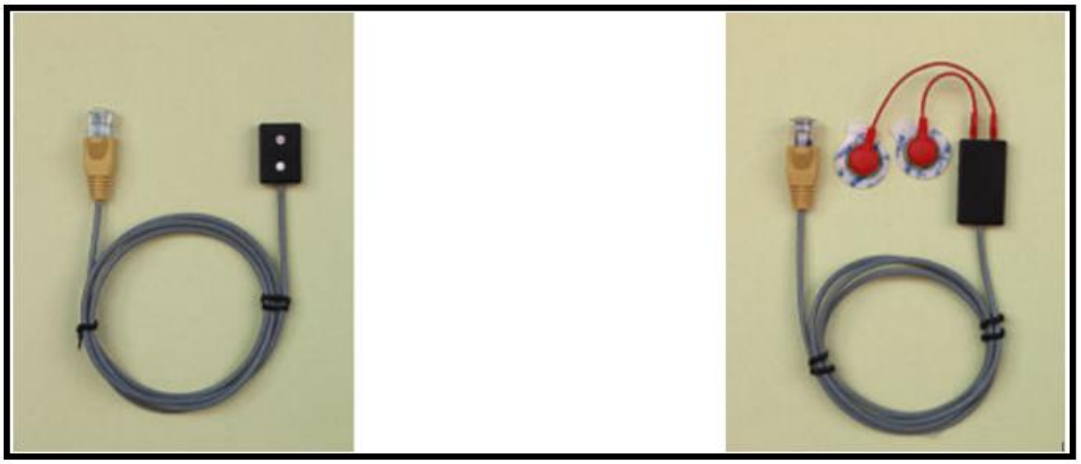

Figure 5.4. On the left, electrode with a fixed geometry. On the right, electrode with variable geometry.

The European SENIAM (Surface Electromyography for the Non-Invasive Assessment of Muscles) recommendations were followed for what concern the location and orientation of the electrodes [52-54]. Following the directive, the electrode should be placed between a motor point and the tendon insertion or between two motor points, and along the longitudinal midline of the muscle. The longitudinal axis of the electrode (which passes through both detection surfaces) should be aligned parallel to the length of the muscle fiber. The electrodes should not be placed in correspondence of the motor point and out of the edges of the muscle. The motor point provides the worst location to detect EMG signal. In this region action potentials travel caudally and rostrally along the muscle fibres. While, outside the edges of the muscle, the electrode detects crosstalk signals from adjacent muscles. Both situations should be avoided. Before the application of the electrodes, what is important to get a good signal and avoid artifact is a proper skin preparation. In fact, the skin was shaved, cleansed with an abrasive paste, and wet with a damp cloth. Probes were placed over rectus

femoris (RF), tibialis anterior (TA), gastrocnemius lateralis (GL), hamstrings (HM) and vastus lateralis (VL). Each subject walked barefoot on the floor for about 5 min at their own pace following an eight-shaped path [55], which includes natural deceleration, reversing, curve and acceleration as shown in *Figure 5.5*.

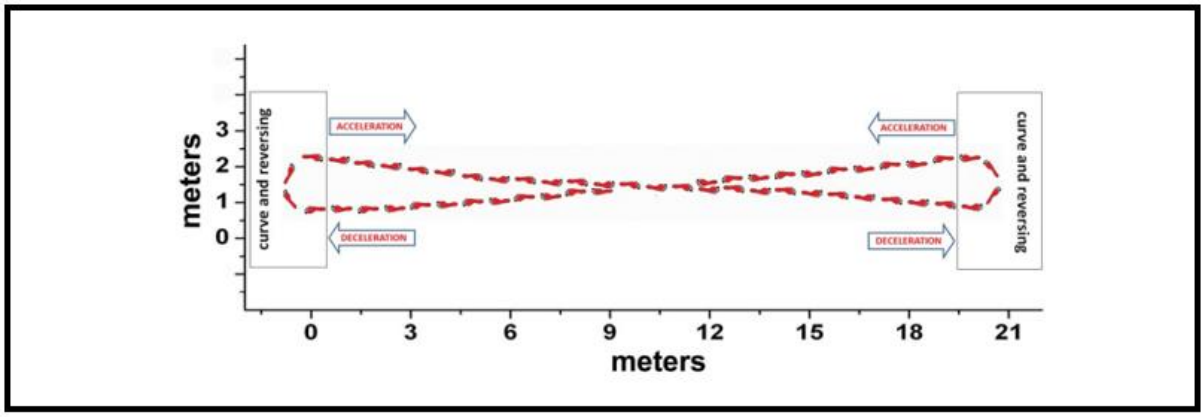

Figure 5.5. Eight-shaped path performed by each subject during walking.

5.2 Signal Pre-Processing

Several steps were followed to pre-process the sEMG data before taking as input to the neural network. The sEMG signals collected from each leg of each subject, before the amplification, had an amplitude ranging from 0 to 10 mV. The frequency spectrum of an EMG signal ranges between 0-500 Hz [56]. Each sEMG signal was amplified, motion artifact and high frequency noise were removed by means of a high-pass filter (finite linear filter FIR: cut-off frequency: 20 Hz) and low-pass filter (finite linear filter FIR: cut-off frequency: 450 Hz) respectively [15]. For each sEMG signal, the envelope was extracted following two step processes: Full-wave rectification and Low-pass filter (second order low-pass Butterworth filter was applied with a cut-off frequency of 5 Hz) [56]. Zero shift was avoided by means of a zero-digital filtering. The last step was the normalization of the sEMG signals (the maximum peak value was considered as reference value) collected from each muscle of each subject in a restricted amplitude ranging between 0 and 1 [15]. In *Figure 2.24* and *Figure 2.25* sEMG signals from Tibialis Anterior, Gastrocnemius, Rectus Femoris, Hamstring, and Vastus Lateralis of both legs of one subject are reported. The basographic signals collected from the foot switches placed under the foot (right foot) were processed to identify the main sub-gait phases: Heel Contact (HC), Flat Foot Contact (FFC), Push Off (PO) and Swing Phase (S). The information derived from the basographic signals were used as ground truth for the neural network.

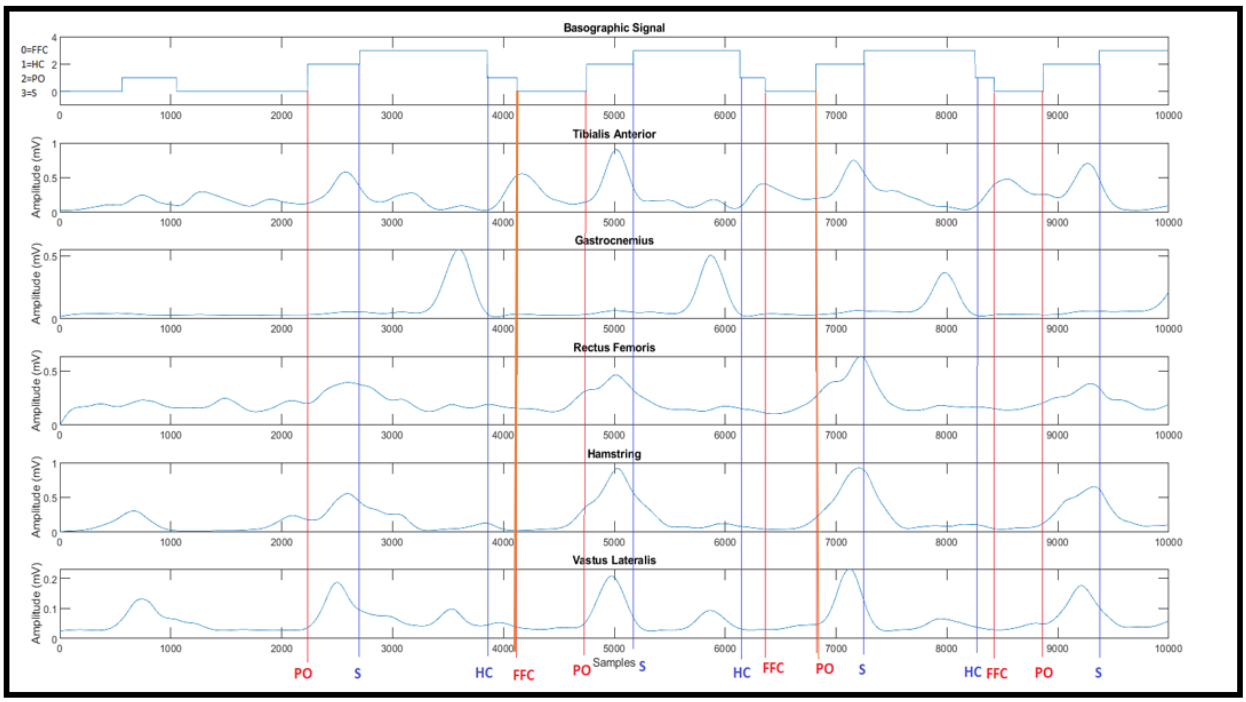

Figure 5.6. Basographic signal of the Left leg and the envelope resulting from the pre-processing of the sEMG of the muscles Left leg are reported. Red lines correspond the instant of time in which Heel Rise and Mid foot event occurred. Heel rise and Mid Foot event were followed by Push Off phase (PO) and Flat Foot Contact (FFC) respectively. Blue lines indicate the instant of time in which Heel Strike and Toe Off occurred. Heel Strike and Toe Offs events were followed by Heel Contact phase (HC) and Swing phase (S). The image shows the first four gait cycles (5 seconds) computed by one subject.

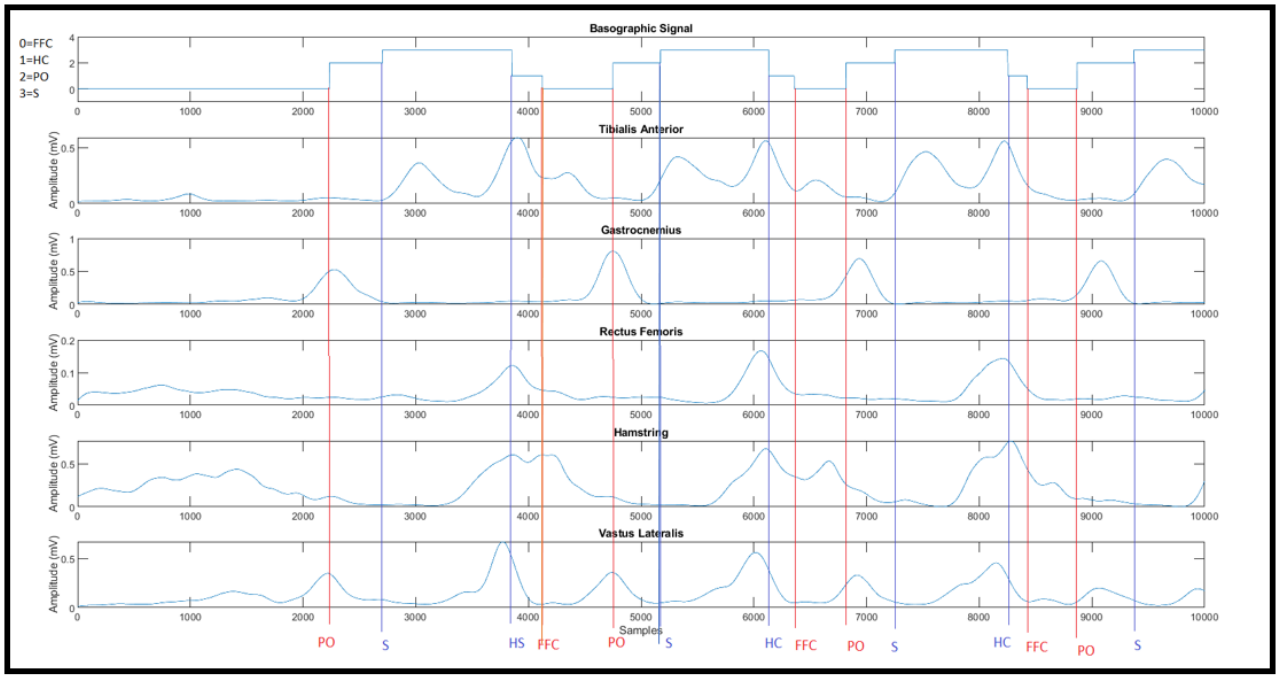

Figure 5.7. Basographic signal of the Right leg and the envelope resulting from the pre-processing of the sEMG of the muscles Right leg are reported. Red lines correspond the instant of time in which Heel Rise and Mid foot event occurred. Heel rise and Mid Foot event were followed by Push Off phase (PO) and Flat Foot Contact (FFC) respectively. Blue lines indicate the instant of time in which Heel Strike and Toe Off occurred. Heel Strike and Toe Offs events were followed by Heel Contact phase (HC) and Swing phase (S). The image shows the first four gait cycles (5 seconds) computed by one subject.

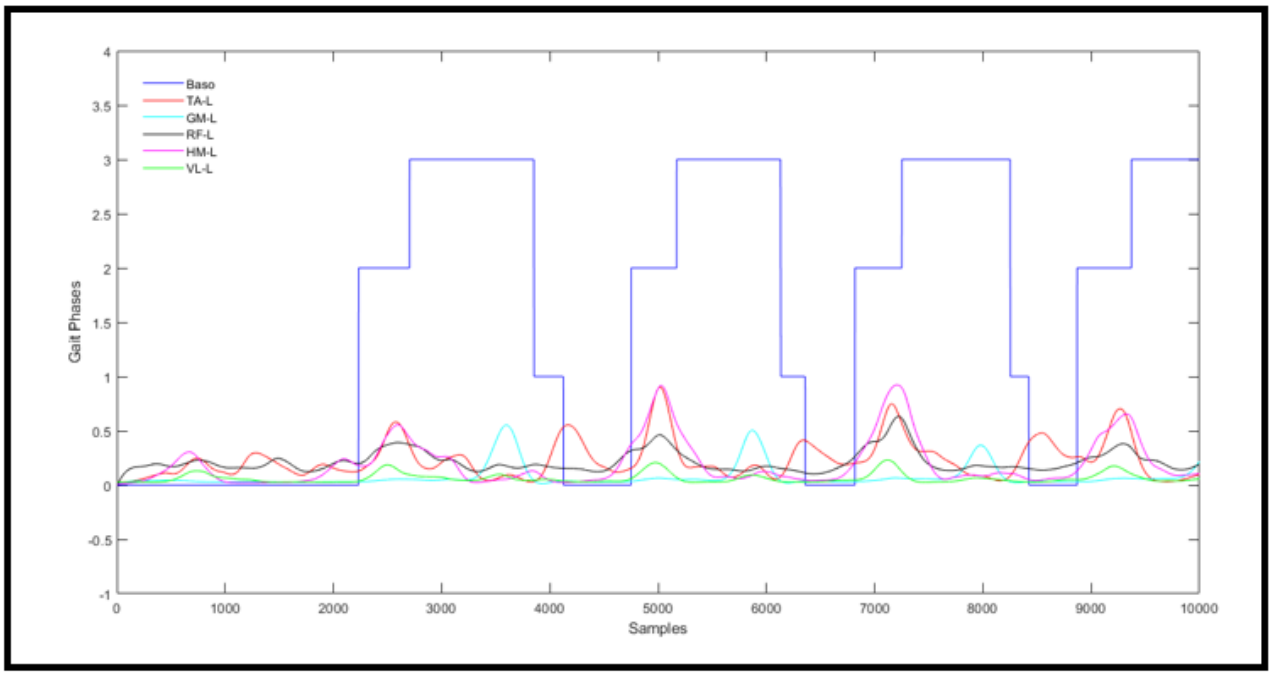

Figure 5.8. Left Foot Basographic Signal (Blue Line) overlapped with sEMG muscles of the left leg related to one subject. The sequence of classes 0 (Flat Foot Contact phase), 2 (Push Off phase), 3 (Swing phase), 1 (Heel Contact phase) define one gait cycle. Typical activity of Left Tibialis Anterior (TA-L), Left Gastrocnemius (GM-L), Left Rectus Femoris (RF-L), Left Hamstring (HM-L), Left Vastus Lateralis (VL-L) during some gait cycles.

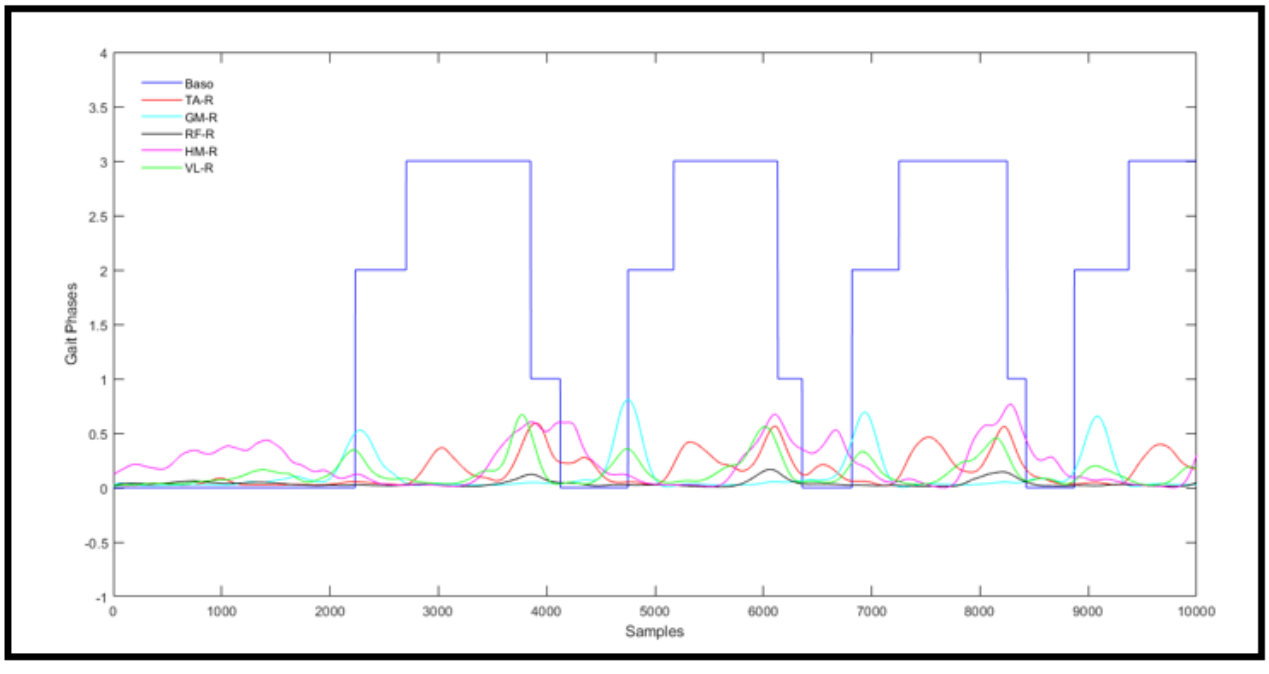

Figure 5.9. Right Foot Basographic Signal (Blue Line) overlapped with sEMG muscles of the right leg related to one subject. The sequence of classes 0 (Flat Foot Contact phase), 2 (Push Off phase), 3 (Swing phase), 1 (Heel Contact phase) define one gait cycle. Typical activity of Right Tibialis Anterior (TA-R), Right Gastrocnemius (GM-R), Right Rectus Femoris (RF-R), Right Hamstring (HM-R), Right Vastus Lateralis (VL-R) during some gait cycles.

5.3 Data Preparation

The sEMG envelopes were used to train the neural network classifier to perform a classification of gait sub-phases (HC, FFC, PO, S phases) and detecting the transitions moment between two phases. In a preliminary study, the first 30.000 samples of sEMG signals of each subject were considered, and a cross-validation using 30 folds was performed, each of which uses data from 29 subjects in training and 1 in test. At each fold, a different subject was used as the test subject. More precisely, the training set collected sEMG envelopes (first 30.000 samples) of each subject (approximately 15 seconds of walking), the test set contained sEMG envelopes of a unique subject considering always the first 30.000 samples. Thus, this first step was done to observe, principally, the training process time work considering partial length sEMG signals of each subject. The final study provided the classification of gait sub-phases (HC, FFC, PO, S phases) and prediction floor foot contact signal, but currently considering the complete sEMG signal acquired during walking on 30 subjects. A cross-validation using 5 folds was performed, each of which uses data from 24 subjects in training set (Learned subjects) and 6 subjects in test set (Unseen subjects). Each fold was composed by different subjects in test set. The information derived from the flat-foot contact signal was used as ground truth for the net and useful to define, in the dataset, the number of gait events (HS, MS, HR, TO) present in each fold both in training and test set. More precisely, the number of gait events identified by the basographic signal is referred to the 24 subjects in training set and the 6 subjects in test set:

- Fold 1 included, in training set, 5568 HS, 5588 MS, 5584 HR, 5596 TO events while the test set was constituted by 1390 HS, 1397 MS, 1396 HR, 1399 TO events.
- Fold 2 included 6444 HS, 6538 MS, 6508 HR, 6560 TO events in training set while the test set include 1611 HS, 1632 MS, 1627 HR, 1640 TO events.
- Fold 3 the training set was constituted by 4780 HS, 4848 MS, 4784 HR, 4804 TO events while the test set included 1195 HS, 1212 MS, 1196 HR, 1201 TO events.
- Fold 4 included, in training set, 5292 HS, 5344 MS , 5332 HR, 5368 TO events while the test set included 1323 HS, 1336 MS, 1333 HR, 1342 TO events.
- Fold 5 included 4908 HS, 4936 MS, 4932 HR, 4936 TO events in training set while the test set included 1227 HS, 1234 MS, 1233 HR, 1234 TO events.

The classification of gait phases and prediction of the basographic signals from sEMG signals were performed on subjects walking on the level ground, in natural conditions as shown in *Figure 5.5*.

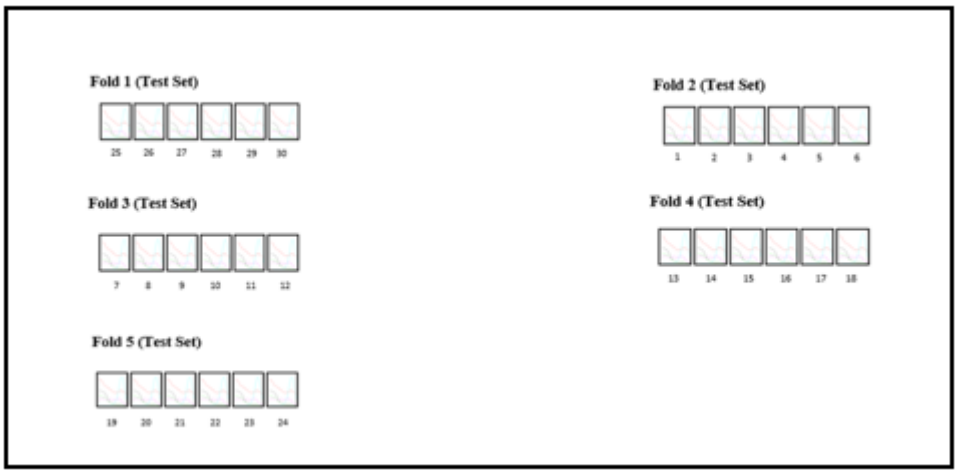

Figure 5.10. Each Fold was constituted by 6 subjects in test set. Fold 1 (Sub 25,26,27,28,29,30), Fold 2 (Sub 1,2,3,4,5,6), Fold 3 (Sub 7,8,9,10,11,12), Fold 4 (Sub 13,14,15,16,17,18), Fold 5 (19,20,21,22,23,24).

The sEMG envelopes were used to train the LSTM neural network, (considered the most suitable for a multi-class classification in this work. Sequence of sEMG envelopes were given as input to the net attempting that it automatically learns relevant hidden features. Classification of gait phases were performed using the open-source web application Jupyter Notebook that uses Python as the programming language. All the sEMG envelope computed for each subject were loaded by means of specific libraries: NumPy and Pandas libraries. For each subject, all ten sEMG time-series signals from rectus femoris (RF), tibialis anterior (TA), gastrocnemius lateralis (GL), hamstrings (HM) and vastus lateralis (VL) of both legs were synchronized so that a vector of 10 elements was constructed for each instant of time. Thus, the dataset consisted of a time-series of sEMG signals. All the data, for the training of the network, of each subject were concatenated by means a specific function defined in the NumPy library to obtain a unique training vector, used to feed the LSTM neural network. The ground truth, represented by the value of the basographic signal was assigned to each input vector and a one hot encoding technique on the target data was performed. The categorical features digit with the value k in [0-3], in which 0 represents Flat Foot Contact phase, 1=Heel Strike phase, 2=Push Off phase and 3=Swing phase, have been encoded into a binary vector with 4 positions, which always has 0 value, except the k-th position where a 1 is assigned. This type of representation is called one-hot encoding (OHE) [57]. Then, in all the experiments, each sEMG signal was split into 500-sample windows (corresponding to 250 ms). A chronological sequence of 500-sample windows was created, the input training size was constituted by windows of 500 samples for each sEMG signal. For instance, considering the first window input, the first element is characterized by the 10 sEMG signals values at the first sample, the second element of the window is characterized by the 10 sEMG

signals values at the second sample and so on. Thus, the training input size was characterized by the following shape: number of windows, 500, 10. The first element corresponds to the total number of the window, the second element represents the amplitude of the window and finally the third element represents the number of sEMG signals collected from each subject considering both the legs. The same procedure has been repeated for all the subjects used as test set.

5.4 Gait sub-phase Classification

Keras libraries were used to load and then work with the net for the classification of gait sub-phases. In all the studies the LSTM neural network used for the classification is available on GitHub [58], it is possible to download it as JSON file and work with it directly opening any note program. The neural network consisted of 3 hidden bidirectional LSTM layers with 32 hidden units (the number of neural units was modified, the original one was composed by 800 units per layer) . Each processing unit corresponds to one neuron. Tanh and Sigmoid optimization functions were defined in each layer. Then, each layer was followed by a dropout layer with a rate of 0.2. A dropout layer helps prevent overfitting (condition in which the net fits too much on a set of data and therefore fail to fit additional data, unknown data for it, or predict future observations reliably) ignoring, randomly, some neurons during training (in this case 20% of neurons) [45]. The input layer was set to take as input 3-dimensional vector in which the first element corresponds to the number of windows, the second element represents the number of samples in each window and finally the third element the values of sEMG signals collected from both legs. The final layer, the one-time distributed layer, was used to classify all the 4 gait sub-phases (Heel Contact, Flat Foot Contact, Push Off and Swing Phase) and the sigmoid function was used as optimization function. Sigmoid function squeezes the k-dimensional vector of arbitrary values into a k-dimensional vector of real values in the range of (0,1) [45]. It aggregates all the answers provided by the previous layers with 4 neurons (k=4, each neuron corresponds to the specific gait sub-phase class); The number of the hidden layers and the number of processing units chosen represents a good compromise between network performance and the training process time work. Then, the model was loaded on Jupyter Notebook application using python libraries. In *Figure 5.11* the overall layout of the neural network for a multi-class classification is reported.

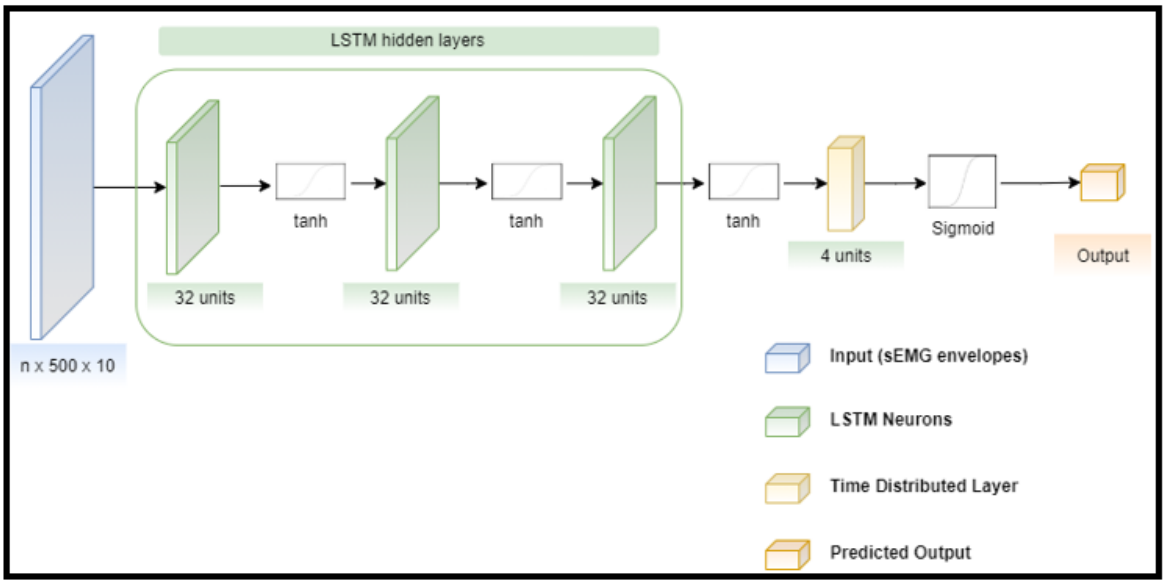

Figure 5.11. LSTM neural network layout for a multiclass classification (4 phases). 3 hidden bidirectional layer and time distributed layer as final layer. For each layer the output shape and the number of parameters is reported. Alle the parameters can be trainable. The terms "n" is not fixed, it represents the number of windows that the neural network takes as input.

Once the model is defined, the neural network was compiled using TensorFlow and keras as backend. In compilation phase, three functions were defined: the optimization function, the loss function and the metrics used to measure the performance of the classification [59]. The first algorithm, while the training process was being performed, was used to update the weights between neuron connections; the second algorithm (loss function) was used by the optimization algorithm to navigate in the space of weights (the process of optimization is also called process of minimization of the loss function). In mathematical optimization, represents the cost associated to an event or value of one variable which its goal is to minimize the error associated to the estimated variable with respect to the actual value of the same variable. Finally, the last algorithm, the metric was used to evaluate the trained model.

The optimizer function used was Adam. Adam optimization is a stochastic gradient descent method that is based on adaptive estimation of first order and second-order moments [60]. Unlike the others stochastic gradient descent methods, the learning rate changes dynamically during training, each time the weight is updated. It works with three parameters: learning rate (α term), first order moment (β_1 term) and second order moment (β_2 term). Specifically, the Adam optimization algorithm uses the advantages of two extensions of stochastic gradient descent AdaGrad and RMSProp. Adaptive Gradient Algorithm (AdaGrad) that keeps a per-parameter learning rate that improves performance on problems with sparse gradients. Root Mean Square Propagation (RMSProp) that also maintains per-parameter learning rates that are adapted based on the average of recent magnitudes of the

gradients for the weight. Instead of adapting the parameter learning rates based on the average first moment as in RMSProp, Adam also makes use of the average of the second moments of the gradients. Specifically, the algorithm calculates an exponential moving average of the gradient and the squared gradient, and the parameters β_1 and β_2 control the decay rates of these moving averages. The initial value of the moving averages and β_1 and β_2 values close to 1 result in a bias of moment estimates towards zero. This bias is overcome by first calculating the biased estimates before then calculating bias-corrected estimates. Within Adam function the parameters as learning rate, β_1 and β_2 were set with their default values. The learning rate is a tuning parameter that determines the step size at each iteration while moving toward a minimum of a loss function. It represents the speed at which a machine learning model learns. It was set to 0.001, β_1 was set to 0.9 and β_2 was set to 0.99 (default values).

The loss function chosen was the categorical cross-entropy. It represents a multi-class logarithmic loss [59]. For instance, considering a target value $t_{i,j}$ and its prediction $p_{i,j}$ from the network ($t_{i,j}$, and $p_{i,j}$ were expressed in one-hot) the error between the target and prediction value is computed by the following equation representing the categorical cross-entropy:

$$L_i = -\sum_j t_{i,j} \log\left(p_{i,j}\right) \qquad 5.1$$

Accuracy was the metric function used to measure the performance of the trained model. It is defined as the ratio between the predictions of the network and the actual values as targets. It is expressed as:

$$Accuracy = \frac{Number\ of\ correct\ predictions}{Total\ number\ of\ predictions} \qquad 5.2$$

Once the model is compiled, the net can be trained. Remaining hyperparameters were set before starting the training process: the number of epochs and the batch size value. The epochs represent the number of times the training process is repeated over the training data. At each iteration the optimizer adjusts the weights so that the loss function is minimized. Batch size is the number of input elements observed before applying the weight update. The number of epochs was set to 20 with a batch size of 32. Furthermore, at each epoch, all the network's weights and training times were saved for all the folds. All the weights, at each epoch, were saved as HDF5 format. In all the studies, training and test set were rigorously separated (There was no point in evaluating a model on a specific data that has already been used for training). In *Figure 5.12*, Train Accuracy and Loss Function development in the first 20 epochs related to a multi-class classification are reported.

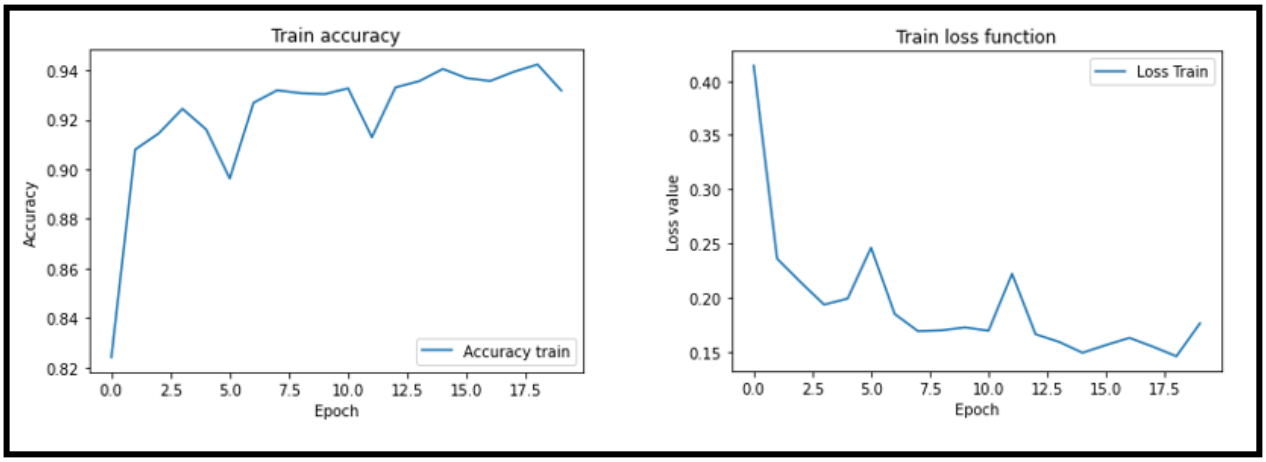

Figure 5.12. Train and Loss function development (first 20 epochs) related to a multi-class classification: Heel Contact, Flat Foot Contact, Push Off and Swing phases.

Once the net is trained, it was used to make predictions on test set by means of the following function:

$$predictions = model.predict\ (data.test) \qquad 5.3$$

This function provided as output, a matrix of predictions with 4 columns (each column represented a specific class) for each element of 500 samples window in dataset used as test set. The matrix of predictions represents, simply, the output of the sigmoid function of the final layer (all the values range between 0 and 1 in each column). The digit with the highest value, given by the sigmoid function, was chosen as prediction and the label 1 was assigned, the other digits, in the remaining 3 columns, were set to 0. Then, in each raw of the matrix of predictions, the positions of the labels 1 were used to construct a categorical prediction vector assigning, in base of the position of the label 1, the values 0,1,2 or 3 corresponding to HC, FFC, PO and S phase respectively. Finally, once the prediction signal was obtained, it was saved as csv file.

5.5 Gait Events Time Detection.

The categorical output of the neural network was chronological arranged to predict the basographic signal. Thus, the output of the network, saved as csv file, was composed of sequences of 1 (Heel Contact phase), 0 (Flat Foot Contact phase), 2 (Push Off phase) and 3 (Swing phase). An algorithm was developed in order to detect the transitions between gait phases, so called gait events: from 3 to 1 (Heel Strike), from 1 to 0 (Mid Foot Strike), from 0 to 2 (Heel Rise) and from 2 to 3 (Toe Off). First, the predicted signal was cleaned in order to remove false phases classified by the network, phases too short according to physiological constraints of the gait cycle [2, 31]. Two threshold values were set: 300 samples (150 ms) for MS, HR and TO; 60 samples (30 ms) for HS. Thus, starting from the first event detected, the following samples, according to the threshold value, were scanned to find and remove all the events which assumes values different from the value of those event. For instance, starting from the first HR event, the following 300 samples were scanned, all the samples which assume value different from 2, hence 0,1 or 3 were removed. Then, the cleaned vector was scanned again to detect the transitions between two phases and the timing of gait events. Finally, the cleaned prediction output was saved as csv file.

At this point, the performance (accuracy) of the classifier in assigning the correct label to the input set containing sEMG segments was measured for the multiclass classification, in assigning 1 for HS phase, 0 for FFC phase, 2 for PO phase and 3 for Swing phase. Anyway, this measure has one limit: even if the accuracy value is high, if the errors are concentrated near the point of transitions, unsatisfactory results will be obtained in terms of time error of gait events. For this reason, a post-processing algorithm was applied to remove false predictions and increase performance. Then, is adopted the following approach to evaluate, used in literature, to evaluate gait events prediction [61, 62]. A temporal tolerance (T) of 300 samples (150 ms) was set, this means that a gait event is considered as a true positive at the time instant t_i if an event of the same type exists in the reference signal (basographic signal) at time t_p such that $|t_p - t_i| < T$. Otherwise, the predicted event is considered as False Positive [61, 62]. For each gait event, precision, recall and F1 Score were measured for all true positive.

Precision is defined as the ratio between the number of true positives divided by the total number of true positive and false positive. It is defined by the following equation:

$$Precision = \frac{TP}{TP + FP} \qquad 5.4$$

Recall is defined as the ratio between the number of true positives divided by the number of true positive summed with false negative. It is defined by the following equation:

$$Recall = \frac{TP}{TP + FN} \qquad 5.5$$

Where:

- TP: True Positives of a predicted event at the time t_i if the same event exists in the reference signal at the time t_p such that $|t_p - t_i| < T$.
- FP: False Positive of a predicted event at the time at the time t_i if the same event doesn't exist in the reference signal.
- FN: False Negative of a predicted event if it doesn't exist but exists in the reference signal.

F1-Score is defined as the harmonic mean between Precision and Recall. It is computed by the following equation:

$$F1\ Score = \frac{2 * Precision * Recall}{Precision + Recall} \qquad 5.6$$

Furthermore, for all true positives, the mean average error (MAE) was computed measuring the temporal distance between the predicted event and the actual one in the reference signal.

5.6 Additional Approach: Stance and Swing Phase Classification

An additional study provided a classification of the two main phases of the gait cycles: Stance and Swing phase and the prediction of the floor foot contact signal (HS and TO events) from sEMG signals. In this case, the first 30.000 samples of each sEMG signal acquired from both legs for each subject were considered and a cross-validation using 30 folds was performed, each of which uses data from 29 subjects in training and 1 in test. Heel Contact, Flat Foot Contact and Push Off phases were included in Stance Phase. The basographic signal values have been modified so that the value 0 corresponds to the Stance phase (HC, FFC, PO labels were set to 0), while 1 to the Swing phase (S label from 3 was set to 1). Then, a binary classification was computed. The label 0 was assigned to each input vector, which signals belong to the Stance phase and 1 if sEMG signals belong to Swing phase. sEMG envelopes were used to feed a LSTM neural network. The net was constituted by 3 hidden LSTM layer followed by a dropout layer. Finally, a one-time distributed layer with 2 processing units was used to classify Stance and Swing phase. The output of the classifier was chronological arranged to predict the basographic signal. It was composed of sequences of 0 (Stance phase) and 1 (Swing phase). A post-processing algorithm, applied on the binary output of the neural network, was used to remove false Swing or false Stance phases classified by the net. Finally, performances in assessing HS and TO events were reported in terms of F1-Score and MAE. *Figure 5.13* shows the overall layout of the neural network for a binary classification.

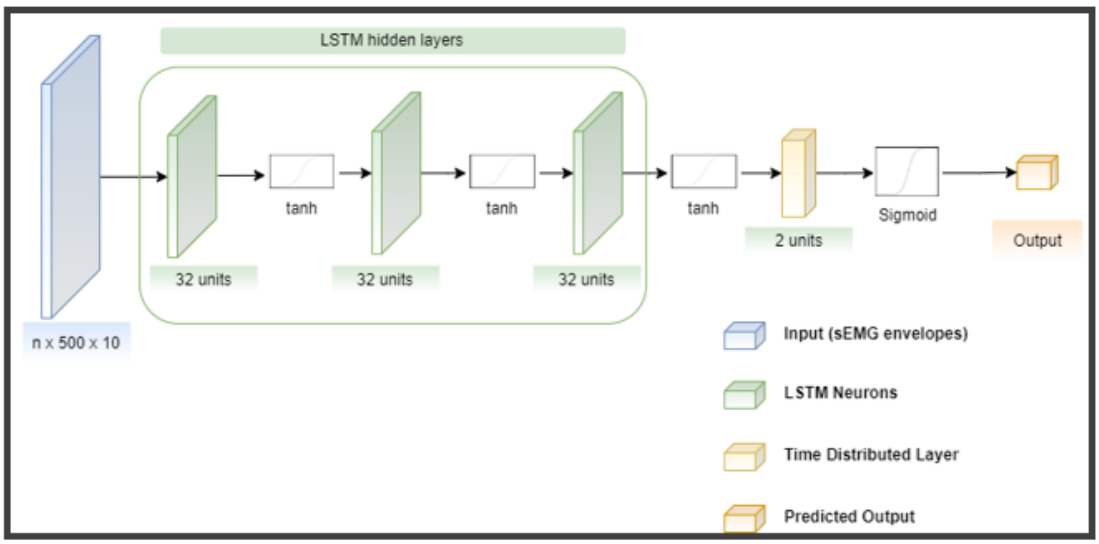

Figure 5.13. LSTM neural network layout for a binary classification (2 phases). 3 hidden bidirectional layer and time distributed layer as final layer. For each layer the output shape and the number of parameters is reported. Alle the parameters can be trainable. The terms "n" is not fixed, it represents the number of windows that the neural network takes as input.

6. Results

The final study provided an attempt to classify gait sub-phases (HC, FFC, PO, S phases) by means of deep learning techniques from sEMG signals acquired from subjects performing a level ground walk. A cross-validation using 5 folds was performed, each of which uses data from 24 subjects in training set (Learned subjects) and 6 subjects in test set (Unseen subjects). *Table 6.1* shows the classification accuracy obtained for Fold 1, Fold 2, Fold 3, Fold 4, and Fold 5 for both Learned subjects and Unseen subjects. Furthermore, the mean classification accuracy and standard deviation (the measure of the grade of dispersion of the values around the mean value) obtained over 5 folds is reported both for Learned subjects and Unseen subjects.

Folds	Learned Subjects	Unseen Subjects
Fold 1	90%	87%
Fold 2	90%	82%
Fold 3	90%	85%
Fold 4	89%	84%
Fold 5	88%	88%
MV (±SD)	89 ± 1.0%	85 ± 2.0%

Table 6.1. Gait phase classification Accuracies (±SD) of Fold 1, Fold 2, Fold 3, Fold 4, and Fold 5 and the averaged one (MV).

One can notice that the average accuracy of gait phases classification (Heel Contact, Flat Foot Contact, Push Off and Swing phase) for subjects in training set is higher than for subjects in test set (89% vs. 85%). Furthermore, looking the value of the Standard Deviation (SD), one can notice a higher variability of accuracy considering unseen subjects set than Learned subjects set (1.0% vs. 2.0%). Anyway, this limited gap (2.0%) on unseen subjects suggests that the LSTM neural network worked well and is able to perform and predict data that it has never seen, unknown to it. Gait sub-phase classification of Fold 1, Fold 2 and Fold 3 performed best on Learned subjects (90%). While the average accuracy on unseen subjects on the five folds varies, which are 87%, 82%, 85%, 84% and 88% respectively. Starting from the result of the classification, the evaluation of the performance in predicting the basographic signal was performed before the application of the post-processing

algorithm on the net output. A temporal tolerance (150 ms) was set, and performance, in terms of MAE and F1-Score in assessing HS, MS, HR and TO events on unseen subjects was computed. *Table 6.2* shows the performance results in predicting gait events for unseen subjects in each Fold. The average prediction error (MAE) computed over the 5 folds on unseen subjects is 20.3 ± 4.4 ms for HS, 32.7 ± 2.5 ms for MS, 20.3 ± 4.4 ms, 51±9.5 ms for HR, 30.38±5.5 ms for TO. Fold 5 performed best in terms of gait events identification on unseen subjects (F1-Score: 90% HS, 81% MS, 83% HR, 83% TO) and prediction error of gait events (MAE: 17.9 ms for HS, 29.3 ms for MS, 40.3 ms for HR, 29 ms for TO). Group of unseen subjects in Fold 2 performed worst in identifying Mid foot strikes (F1-Score 72%), Heel Rise (F1-Score 72%) and Toe Off events (F1-Score 76%). In general, as for prediction accuracy of each gait event, Heel Strike event performed best (F1-Score 90 ± 4.0%). Toe Off event is also good (F1-Score 86 ± 4.0%) except for low value of performance in Fold 2. Mid Foot Strike event and Heel rise event have the lowest performance with none of accuracies achieved 90% and have the lowest values of table on Unseen subjects of Fold 2.

		Heel Strike	Mid-Foot Strike	Heel Rise	Toe Off
Fold 1	F1-Score	91%	82%	82%	90%
	MAE (ms)	19.89	32.24	44.52	21.96
Fold 2	F1-Score	88%	72%	72%	76%
	MAE (ms)	27.59	36.74	51.94	33.14
Fold 3	F1-Score	97%	96%	85%	97%
	MAE (ms)	16.08	33.15	65.15	34.33
Fold 4	F1-Score	85%	81%	86%	82%
	MAE (ms)	20.02	31.49	53.47	33.48
Fold 5	F1-Score	90%	81%	83%	83%
	MAE (ms)	17.93	29.98	40.34	28.99
MV (± SD)	F1-Score	90 ± 4.0%	80 ± 12.0%	82 ± 6.0%	86 ± 8.0%
	MAE (ms)	20.30±4.38	32.72±2.54	51.08±9.52	30.38±5.14

Table 6.2. F1-Score (±SD) and Mean Average Error (MAE) measured on unseen subjects of each Fold. The evaluation of the predicted gait events is performed considering the prediction signal directly coming out of the neural network.

Considering the mean average error value, one can notice that net shown more difficulty in predicting HR events. In fact, the highest time prediction error occurred for HR event (51.08 ± 9.52 ms).
As already said in Section 5.5, the output of the network is influenced by false phases classified by the net. A post-processing algorithm has been applied to remove false phases and phases too short according to physiological constraints of the gait cycle [2, 31]. Then, the cleaned vector was scanned to detect the transitions between two phases and the timing of gait events. *Table 6.3* shows the performance in terms of F1-Score and MAE in identifying and predicting gait events HS, MS, HR and TO once the post processing algorithm is applied. The table reports the results related on Unseen subject in each Fold. Comparing the results reported in *Table 6.2* with the results reported in *Table 6.3*, one can notice that the performance in identifying gait events is augmented once the post-processing algorithm is applied: F1-Score HS: 90% vs 92%, F1-Score HR: 82% vs 90%, F1-Score TO: 86% vs 97% and F1-Score MS:80% vs 96% respectively. For what concern the prediction time error expressed as the time distance between the instant of time in which the event takes place and the estimated one (MAE), it remained almost unchanged, more precisely, post-processing output show a slight increase of time error prediction: MAE HS: 20.3 ms vs 20.6 ms, MAE HR: 51.1 ms vs 53.8, MAE TO: 30.4 ms vs 30.9 ms and MAE MS: 32.1 ms vs 35 ms. One can notice that, also in this case, Fold 5 performs best in terms of gait event identification and gait event time error prediction. The F1-Score reaches values near to 100% for HS (98%), MS (98%), and TO (98%) event identification. HR event is also good reaching a F1-Score of 94%. Also in the case, in this specific fold, the time error prediction is slightly augmented (MAE HS: 19.4 ms, MAE MS: 32.5 ms, HR:44.1, TO: 30.2). Unlike the previous case, the performance in identifying gait events on Unseen subjects in Fold 2 is greatly increased and in line with the performances obtained on Unseen subjects of the other folds. Furthermore, one can notice that the best performance, in terms of F1-Score, obtained over the 5 folds are performed by MS (F1 Score 96%) and TO (F1 Score 97%) events, in contrast with the results shown in *Table 3.2* in which HS and TO events shown the best performance. Anyway, HS and HR event obtained a good performance achieving an F1-Score of 92% and 90% respectively. For what concern the time error prediction (MAE), the best performances are achieved by HS and TO events with an average time error over the 5 folds of 20.7 ± 4.8 ms and 30.9 ± 5.0 ms respectively. More detailed results (F1-Score and MAE values) related to each Unseen subject in each Fold are reported in Appendix.

		Heel Strike	Mid-Foot Strike	Heel Rise	Toe Off
Fold 1	F1-Score	88%	94%	93%	99%
	MAE (ms)	17.93	41.50	50.45	22.45
Fold 2	F1-Score	89%	98%	86%	95%
	MAE (ms)	28.47	34.12	54.34	33.26
Fold 3	F1-Score	98%	97%	85%	97%
	MAE (ms)	16.08	33.15	65.15	34.32
Fold 4	F1-Score	89%	94%	89%	96%
	MAE (ms)	21.39	34.06	54.97	34.09
Fold 5	F1-Score	98%	98%	94%	98%
	MAE (ms)	19.44	32.47	44.07	30.17
MV (± SD)	F1-Score	92 ± 4.0%	96 ± 2.0%	90 ± 4.0%	97 ± 2.0%
	MAE (ms)	20.66±4.78	35.06±3.66	53.80±7.69	30.86±4.98

Table 6.3. F1-Score (±SD) and Mean Average Error (MAE) measured on unseen subjects of each Fold. The evaluation of the predicted gait events is performed on the post-processing signal.

Figures 6.1, *6.2* and *6.3* show an example of prediction of the foot floor contact signal (blue line) provided by this approach compared with the ground truth (red line) represented by the basographic signal of three unseen subjects (subjects 19, 20, 21) in Fold 5. The figures show the predictions made in the first 15 seconds. The sequence of classes 1, 0, 2, 3 represent one gait cycle corresponding to a series of Heel Contact, Flat Foot Contact, Push Off and Swing phases respectively. Gait events are defined as transition moments between gait phases. One can notice that this approach, provide a good prediction of the flat foot contact signal, each predicted gait cycle overlaps with the reference one also in the presence of irregular walking activity (subjects walked on the ground performing an eight-shape path). *Figure 3.1* shows the prediction of the ground flat foot contact signal of subject 19. A good prediction is obtained for this specific subject, almost all gait events are correctly identified (F1 Score HS: 95%, F1 Score MS: 98%, F1 Score HR: 91%, F1 Score TO: 96%) with an average time error of prediction (MAE) of 27.0 ms for HS, 47.2 ms for MS, 30.0 ms for HR, 23.6 ms for TO event. One can notice that in the first 15 seconds all the gait events are correctly predicted, gait phases (Heel

Contact, Flat Foot Contact, Push Off and Swing phases) are well defined except in the first gait cycle in which an additional swing phase has been classified immediately after the previous Heel contact phase. Anyway, the predicted signal is able to clearly follow the ground truth represented by the foot floor contact signal. Note that Heel Contact phase is the shortest phase, it corresponds to only 2% of gait cycle.

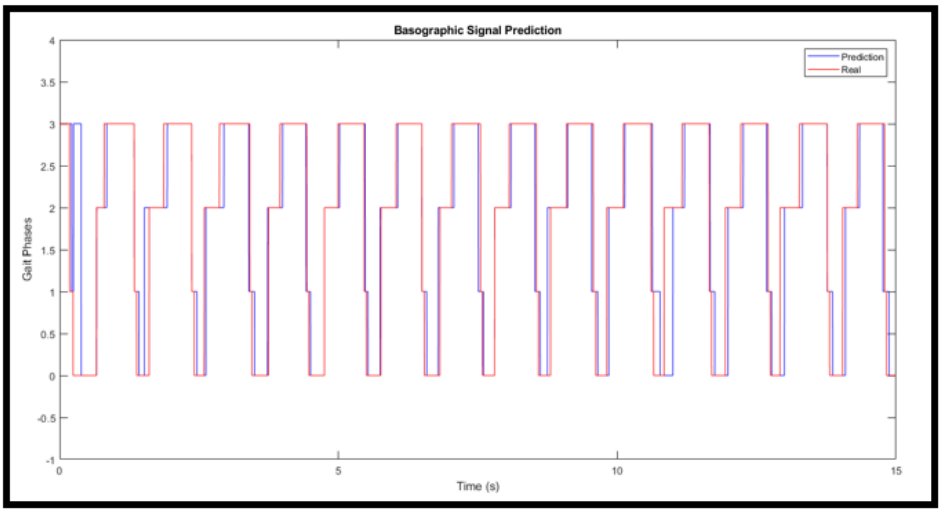

Figure 6.1. Unseen subject 19 in Fold 5. Blue Line predicted signal. Red line reference one (floor foot contact signal). Class 0=FFC phase, Class 1=HC phase, Class 2=PO phase, Class 3=Swing phase. HS event between class 3-1, MS event between class 1-0, HR event between class 0-2, TO event between class 2-3.

Figure 6.2 shows the prediction of the ground flat foot contact signal of subject 20. An excellent prediction is obtained for this specific subject, almost all gait events are correctly identified, in particular TO events are all correctly predicted (F1-Score HS: 99%, F1-Score MS: 99%, F1-Score HR: 96%, F1-Score TO: 100%) with an average time error of prediction (MAE) of 18.4 ms for HS, 38.5 ms for MS, 60.6 ms for HR, 32.8 ms for TO events. In the first 15 seconds shown in the figure, one can notice that a good prediction of HS, MS, HR and TO events occur (predicted and foot floor contact signals are almost completely overlapped), gait phases (Heel Contact, Flat Foot Contact, Push Off and Swing phases) are correctly classified in all gait cycles. Unlike the previous subject, one can notice the predicted timing error of HR events in some gait cycles especially in the first one. However, this is a very small error since also in this case the predicted signal is able to faithfully follow the reference signal as for the previous subject.

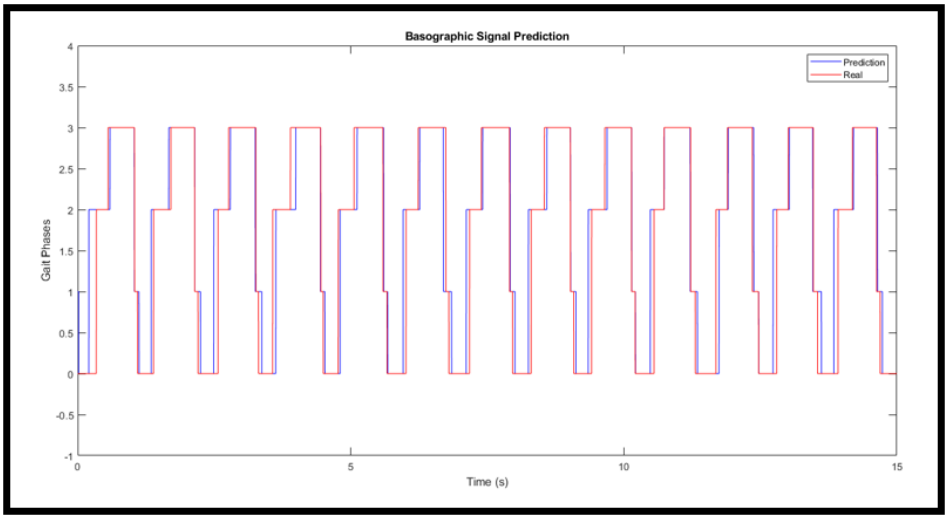

Figure 6.2. Unseen subject 20 in Fold 5. Blue Line predicted signal. Red line reference one (floor foot contact signal). Class 0=FFC phase, Class 1=HC phase, Class 2=PO phase, Class 3=Swing phase. HS event between class 3-1, MS event between class 1-0, HR event between class 0-2, TO event between class 2-3.

Figure 6.3 shows the prediction of the ground flat foot contact signal of subject 21. An excellent prediction is obtained for this specific subject, almost all gait events are correctly identified, in particular TO events are all correctly predicted (F1-Score HS: 97%, F1-Score MS: 99%, F1-Score HR: 96%, F1-Score TO: 97%) with an average time error of prediction (MAE) of 21.7 ms for HS, 19.7 ms for MS, 30.7 ms for HR, 33.6 ms for TO events. In the first 15 seconds shown in the figure, one can notice that a good prediction of HS, MS, HR and TO events occur (predicted and foot floor contact signals are almost completely overlapped). In one gait cycle there is an additional heel contact phase that should not be there, so a false positive event (HS) has been detected.

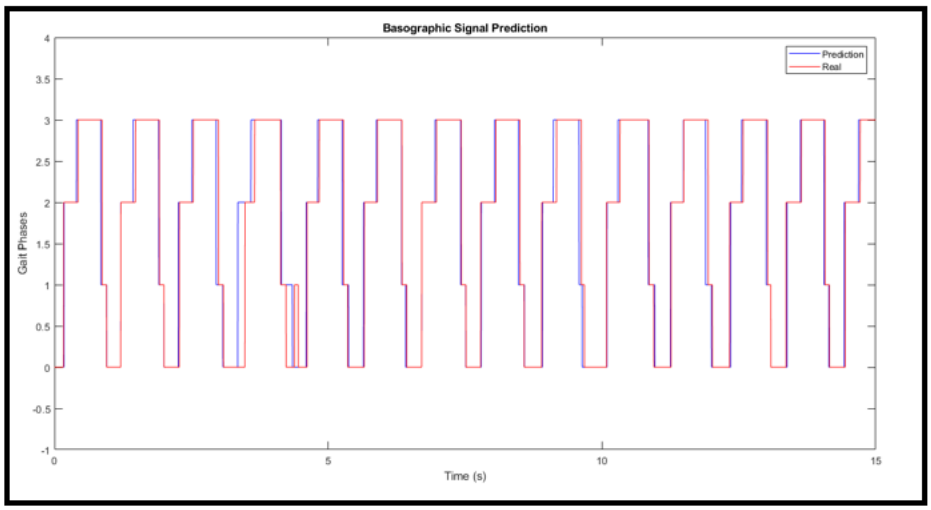

Figure 6.3. Unseen subject 21 in Fold 5. Blue Line predicted signal. Red line reference one (floor foot contact signal). Class 0=FFC phase, Class 1=HC phase, Class 2=PO phase, Class 3=Swing phase. HS event between class 3-1, MS event between class 1-0, HR event between class 0-2, TO event between class 2-3.

In the additional study a binary classification was performed. sEMG envelopes were used to feed a LSTM neural network to classify the main gait phases: Stance and Swing phase. *Table 6.4* shows the average classification accuracy (±SD) obtained over the 30 folds on Learned subjects and Unseen subjects. The net was able to classify the main gait phases with an average accuracy of 95 ± 0.4% on Learned subjects and 93 ± 3.0% on unseen subjects.

	Learned Subjects	Unseen Subject
Accuracy (±SD)	94 ± 0.4%	93 ± 3%

Table 6.4. Average classification Accuracy (±SD) obtained over the 30 folds for Learned Subjects and Unseen Subjects.

One can notice that the average accuracy of gait phases classification (Stance and Swing phase) for subjects in training set is higher than for subjects in test set (89% vs. 85%). Furthermore, looking the value of the Standard Deviation (SD), one can notice a higher variability of accuracy across the 30 folds considering unseen subjects set than Learned subjects set (0.4 vs. 3.0). Also in this case, the limited gap, around 3.0 %, on unseen subjects suggests that the LSTM neural network worked well and was able to classify data that it has never seen. The performance in detecting HS and TO events was measured on post-processing net output in terms of F1-Score and MAE. Over the 30 folds, on unseen subjects, HS events were predicted in 25.14±12.28 ms and TO events were predicted in 35.32±14.37 ms with an F1-Score of 95 % ± 6.0 and 93 % ± 7.0 respectively (*Table 6.5*). The approach, followed in this study, allows to reach better performances in predicting Heel Strike events rather than Toe Off events.

MV (±SD)	Heel Strike	Toe Off
F1-Score	95 ± 6.0%	93 ± 7.0%
MAE (ms)	25.14±12.28	35.32±14.37

Table 6.5. Evaluation of Prediction of basographic signal. Average MAE and F1-Score (±SD) results obtained over the 30 folds on unseen subjects.

7. Discussion and Conclusion

The goal of this study is to propose a novel approach for classifying the main gait sub-phases (Heel Contact, Flat Foot Contact, Push Off and Swing phase) and assessing HS, MS, HR and TO events by means of a deep learning approach based on the analysis of sEMG signals acquired from five muscles of both legs during walking. Foot-switches signals were adopted as the ground truth since it is a very accurate approach for assessing spatial-temporal parameters and allows to acquire numerous consecutive strides [19]. A LSTM recurrent neural network composed by three hidden layers with 32 units was chosen. A one-time distributed layer was chosen as output layer to classify the four gait sub-phases. All the inputs data are arranged in a temporal sequence. Considering the complexity of classification of sub phases due to the high variability of temporal and spatial parameters of the sEMG signals in natural walking condition, the LSTM recurrent neural network was considered more suitable to the aim of this study. In general, time and frequency domain features are extracted to train the model in order to classify EMG signals from lower-limb muscles [63]. However, the choice of the feature could affect the performance of classification. For this reason, the present study directly used the envelope of sEMG signal to train the networks, attempting to automatically learn relevant higher level (hidden) features, following the procedure proposed in [15]. The training process was repeated 5 times, each time using different six subjects as test set. Thus, a cross-validation with 5 folds was performed. The *Table 6.1* shows the average sub phase classification accuracy over 5 folds (±SD) of 89 ± 1.0% for Learned Set and 85 ± 2.0% for test set. On unseen subjects a reduction of accuracy is detected, and as expected, the standard deviation is higher, indicating a large variability of classification for subjects not used during training phase. Anyway, the classification accuracy achieved on unseen subjects is still ≥ 85%, suggesting that the model is able to perform a reliable gait sub-phase classification even testing on subjects that it has never seen before. Accuracy values < 90% are likely due to different factors. The main one is that the sEMG dataset was quite imbalanced. In fact, the sEMG data were segmented into 4 classes, following the physiological definition of gait sub-phases; thus, each class had a different duration (i.e., different number of samples to classify). The Swing phase covered the biggest part of the dataset (it corresponds to the 40-45% of the gait cycle) followed by flat foot contact phase (20-30% of the gait cycle), push off (15-25% of the gait cycle) and Heel contact phase (the shortest phase corresponding to the 5-10% of gait cycle). This issue could be improved by augmenting the dataset and making it more balanced. The second factor is due to the large variability of the sEMG and foot-floor-contact signals that could affect the performance of the classifier. The subjects, indeed, followed an eight shaped path on the ground during the experimental protocol and this introduce gait variability such as number of steps and cadence, walking speed and

changes in sEMG activation, due to curves, reversing, acceleration, deceleration with respect to the treadmill walking. The impact of this issue has been partially limited by using a great amount of data to train the model (ten sEMG signals were acquired from both legs per subject and around 11.000 gait cycles considering the 24 subjects in training).

The identification of gait events was performed both directly on the net output and after an effective post-processing of model output, ensuring values of F1-Score above 90%. *Table 6.2* and *Table 6.3* show a comparison between the prediction of gait events before the application of the post-processing algorithm on model output and the prediction of gait events after an effective post-processing of model output. In the first case (no post processing), a mean F1-Score over the 5 folds on unseen subjects of $90 \pm 4.0\%$, $80 \pm 12\%$, $82 \pm 6.0\%$, $86 \pm 8.0\%$ was reached in identifying HS, MS, HR and TO events respectively (*Table 6.2)*. Furthermore, a mean MAE over the 5 folds of 20.3 ± 4.4 ms, 32.7 ± 2.5 ms, 51.1 ± 9.5 ms, 30.4 ± 5.1 ms is achieved in predicting HS, MS, HR, TO events respectively. As expected, gait events within the stance phase such as mid foot strike and heel rise events performed worst respect to heel strike event, representing the transition moment between swing and stance phase, and toe off event, representing the transition moment between stance and swing phase. Anyway, prediction error up to 50 ms can be considered acceptable from the clinical point of view because 50 ms corresponds to a percentage of gait cycle < 5%. In the second case application of the post-processing procedure), the predicted signal was cleaned in order to remove false positives in phase classification and phases too short according to physiological constraints of the gait cycle [2, 31]. This approach allows to achieve better performances in terms of F1-Score, it allows significant improvement, especially for Mid foot strike events, of 12% reaching an F1-Score of 96%. Anyway, better performances in terms of F1-Score are achieved by all gait events with respect to the previous case: F1-Score HS: 92% (+ 2%), F1-Score HR: 90% (+ 8%), F1-Score TO: 97% (+ 11%), and F1-Score MS: 96% (+ 16%), respectively (*Table 6.3)*. It is important to notice that also SD values decreased (from 12 to 2% for MS, from 6 to 4% for HR and from 8 to 2% for TO) except for HS event which remained invariant. This suggests that the introduction of a post-processing procedure allows to reach a high repeatability of prediction quality among the five folds. Concomitantly, MAE values remain practically unaltered between the two approaches. One could notice that the performances of this approach mainly deteriorate in detecting HR events (gait event which precedes the push off phase) showing a prediction time error higher than that achieved by other gait events (53.8 ms). Although the heel rise event is the hardest to predict, the MAE remains around 50 ms, hence may be acceptable from a clinical point of view. Moreover, it is important to remind that these performances are achieved in a condition of high variability of foot floor contact due to the eight shape path followed by each subject. In literature, there are some studies that performed a

classification of gait sub phases by means of a machine learning approach using sEMG only [10,11,29,30,64]. The study presented in [29] achieves the better results in terms of only mean classification accuracy of six gait sub phases using a machine learning approach. However, none of these studies attempted to predict all gait events (HS, MS, HR and TO), thus the prediction error of gait events is not available for comparison. Furthermore, in these studies the experiments were performed on few subjects who walked on treadmill yielding more performing the classification process of gait sub phases. Thus, to date there are no better all gait event predictions (HS, MS, HR and TO) than those obtained in this research.

In Appendix detailed performances in terms of F1-Score and MAE are reported for each Unseen subject in each fold. It is possible to notice that there is not a great variability around the mean value in all gait events; only few subjects distinguish from the mean values. More precisely, only subjects 2 and 5 in Fold 2 present a higher time error (MAE) of 95 ms and 97 ms for HR prediction, respectively. However, the net achieved on the same subjects excellent values in the predictions of the other transition instants, in particular on HS and MS events with a time prediction error (MAE) of 30.1 ms on subject 2 and 26.1 on subject 5 for HS event and a MAE of 37.9 ms on subject 2 and 21.0 ms on subject 5 for MS event. Otherwise, there are several good-performing predictions of gait events where MAE for HR event remains lower than 50 ms. Excellent performances are achieved, for example, on subjects 12 (Fold 3), 13 (Fold 4), 21 (Fold 5) and 28 (Fold 1). More precisely, subject 12 shows the best performance in terms of MAE in detecting HS event (10.4 ms), subjects 13 obtained the bast MAE in detecting MS (17.8 ms), subject 21 shows the best MAE in identify HR events (30.7 ms) and subject 28 performed best not only in detecting TO events (MAE: 17.7 ms) but performed best also in terms of F1-Score achieving 100 % for all gait events. The approach faced in this study shown its reliability especially in identifying Heel strike, Mid foot strike and Toe off events with a mean prediction error (MAE) of 20.6 ms, 35.1 ms and 30.9 ms respectively. Anyway, these performing results were achieved thanks to the high number of gait cycles considered per subjects (around 400-500 gait cycles per subject) and the five EMG signals acquired from each leg. In future projects it is possible to try to reduce the number of Emg signals acquired from each subject in order to reduce the invasiveness of the experimental protocol; this study has demonstrated that by means a deep learning approach, is possible to predict gait events on subjects performing a natural walking without the need of external sensors such as IMUs devices, stereophotogrammetric systems or foot switches sensors. Future projects could focus on reducing the number of EMG signals acquired from each subject in order to reduce the invasiveness of the experimental protocol.

A further effort has been done in the present study: we tried also to test the ability of the approach in binary classifying the two main gait phases (Stance and Swing phases) and predict the transition

moment between them (HS and TO events). *Table 6.4* shows the average classification accuracy (±SD) obtained over 30 folds on Learned subjects and Unseen subjects. The LSTM neural network was able to classify the main gait phases with an average accuracy of 95 ± 0.4% on Learned subjects and 93 ± 5.0% on Unseen subjects. One can notice that SD is higher for unseen subjects than Learned subjects. Notice that, the average accuracy across the 30 folds do not show a significant variability (very small, around 0.4%). It may be due the subdivision of data between training set and test set: in each fold only one subject was used as test set, while the data of the other 29 subjects were used as training set. The higher variability on Unseen subjects (around 5.0%) could be because the first 30.000 samples of each sEMG signal were considered to train the neural network. Thus, considering only few samples of sEMG data made the classification harder on subjects that the net has never seen. The performance in detecting HS and TO events was measured after post-processing in terms of F1-Score and MAE. Over the 30 folds, MAE was 25.14±12.28 ms in HS prediction and 35.32±14.37 ms in TO prediction. Correspondent F1-Score values were of 95 ± 6.0% and 93 ± 7.0% respectively. To test the reliability of HS and TO predictions, the results provided by this additional study were compared to the results in predicting HS and TO events achieved in literature where a stance and swing classification was performed by deep learning approaches based on only sEMG signals. In [14] five time-domain features were extracted from electromyographic signals to feed a single hidden layer neural network to classify stance and swing phases. The data were acquired from eight subjects performing walking on a treadmill for about 5 seconds. Despite this, the results reported in this approach shown a mean average error of 35 ± 25 ms for HS and 49 ± 15 ms for TO. Thus, the approach faced in this additional study performed better in terms of time error compared to the results obtained in [14] confirming that the LSTM neural network succeeded in learning hidden features relevant to the task to be performed compared to the features used in the previous study. The best results were achieved in [15] where sEMG envelopes were used to feed a multilayer perceptron neural network to classify stance and swing phases. sEMG data were acquired from 23 subjects performing walking on the level ground following an eight shape path. The sEMG signals were acquired from 4 leg muscles. A cross validation with 23 folds was performed using 22 subjects in training set and a different subject as test set. The evaluation of performance was measured in terms of F1-Score and Mae. On unseen subjects, the study achieved a mean time prediction error over the 30 folds of 21.6 ± 7.0 ms for HS and 38.1 ± 15.2 ms for TO. In [18] the same group of researchers proposed an intra-subject approach for stance and swing classification and the prediction of gait events by means of deep learning techniques based only on sEMG signals. The sEMG signals were acquired from 5 leg muscles in about 10.000 gait cycles from 23 healthy subjects. They demonstrated that an intra-subject approach was able to achieve better performances than the inter-subject one in HS and TO predictions. A time

prediction error of 14.4 ± 4.7 ms for HS and 23.7 ± 11.3 ms for TO events was achieved. The approach faced in this additional study is an inter subject approach, in which sEMG data of different subjects were used to feed a recurrent neural network, a net more complex to train respect to a multilayer perceptron neural network. Anyway, the results obtained in this additional study can be considerable in line with that reported in [14,15,18] and support the reliability of the results provided by the same model in classifying 4 gait sub-phases and predicting four gait events.

In conclusion, the present research proposed a novel method to classify the main four gait sub-phases and predict the transition instants between them by means of a deep learning approach based on the interpretation of only sEMG signals acquired during level ground walking. More precisely, sEMG envelopes were used to feed an artificial neural network attempting that the net learns hidden relevant features. Good performances are achieved in terms of F1-Score and MAE in predicting Heel Strike, Mid foot Strike, Heel Rise, and Toe off events. From the clinical point of view, the results obtained in this research, can be considerable encouraging because by means of a deep learning approach based only on sEMG signals is possible to carry out a gait analysis on patients performing a natural walking without the need of further external sensors to measure foot-floor-contact signal, such as IMUs devices, or foot switches sensors, thus reducing the invasiveness, the time consumption, and the cost of the experimental set-up. Automatic recognition of gait phases and detection of gait events could also be important to drive power limb exoskeleton or assistive devices that have been developed in the last decades aiming at helping humans to enhance their walking ability [65, 66]. In future research, an attempt could be to reduce the number of sEMG signals acquired from lower limbs, passing from five monitored muscles to four, and observe how much the performance is affected in predicting gait events in order to further simplify the experimental set-up.

References

1. A. Alamdari, V.N Krovi, "A review of Computational Musculoskeletal Analysis of Human Lower Etremities", *in Human Modelling for Bio-Inspired Robotics*, *pp- 37-73,* 2017.
2. L.M. Silva, N. Stergiou, "The basics of gait analysis", *in Biomechanics and Gait Analysis*, *pp. 225-250,* 2020.
3. M. Lampereur, F. Rouseeau, O. Rémy-Néris, P. Christelle, L. Houx, G. Quellec, S. Brochard, "A new deep learning-based method for the detection of gait events in children with gait disorders: Proof-of-concept and concurrent validity", *Journal of Biomechanics*, *98(1):109490*, 2020.
4. J.X.J. Zhang, K. Hoshino, "Implantable and wearable sensors", *in Molecular Sensors and Nanodevices 2nd Edition, pp. 489-545*, 2019.
5. N. Jarrasse, C. Nicol, A. Touillet, F. Richer, N. Martinet, J. Paysant, J. B. de Graaf, "Classification of phantom finger, hand, wrist, and elbow voluntary gestures in transhumeral amputees with semg", *IEEE Transactions on Neural Systems and Rehabilitation Engineering, vol. 25, no. 1, pp. 68–77*, 2017.
6. D. Feng, L. Dai, W. Chang, Z. Chen, C. Zhu, and W. Li, "semg-based identification of hand motion commands using wavelet neural network combined with discrete wavelet transform", *IEEE Transactions on Industrial Electronics, vol. 63, no. 3, pp. 1923–1934*, 2016.
7. Q. C. Ding, J. D. Han, and X. G. Zhao, "Continuous estimation of human multi-joint angles from semg using a state-space model," *IEEE Transactions on Neural Systems & Rehabilitation Engineering a Publication of the IEEE Engineering in Medicine & Biology Society*, *vol. PP, no. 99, pp. 1–1*, 2016.
8. J. Taborri, E. Palermo, S. Rossi, P. Cappa, "Gait Partitioning Methods: A systematic Review", *Sensors (Basel), 16(1):66,* 2016.
9. F. Di Nardo, C. Morbidoni, A. Cucchiarelli, S. Fioretti, "Recognition of Gait Phases with a Single Knee Goniometer: A Deep Learning Approach", *Electronics, 9(2), 355*, 2020.
10. M. Meng, Q. She, Y. Gao, and Z. Luo, "Emg signals based gait phases recognition using hidden markov models", *in IEEE International Conference on Information & Automation, pp. 852-856*, 2010.
11. C.D Joshi, U. Lahiri, N.V. Thakor, "Classification of Gait Phases from Lower Limb EMG: Application to Exoskeleton Orthosis", *IEEE Point-of-Care Healthcare Technologies*, *pp. 228-231*, 2013.
12. N. Nazmi, M. Abdul Rahman, M.H.M. Ariff, S. Ahmad, "Generalization of ANN Model in Classifying Stance and Swing Phases of Gait using EMG Signals*", In Proceedings of the IEEE-EMBS Conference on Biomedical Engineering and Sciences, pp. 461-466,* 2018.
13. J. Ziegier, H. Gattringer, A. Mueller, "Classification of Gait Phases Based on Bilateral EMG Data Using Support Vector Machines", *In Proceedings of the IEEE RAS and EMBS International Conference on Biomedical Robotics and Biomechatronics, pp. 978-983,* 2018.
14. N. Nazmi, A. Rahaman, M. Yanamoto, S. Ahmad, "Walking gait event detection based on electromyography signals using artificial neural network", *Biomedical Signal Processing and Control, pp. 334-343*, 2019.
15. C. Morbidoni, A. Cucchiarelli, S. Fioretti, F. Di Nardo, "A deep Learning Approach to EMG-Based Classification of Gait Phases during Level Ground Walking", *electronics*, *8(8), 894*, 2019.
16. J. Kamruzzaman, R.K. Begg, "Support vector machines and other pattern recognition approaches to the diagnosis of cerebral palsy gait", *IEEE Trans Biomed Eng*, *53(12 Pt 1):2479-90,* 2006.
17. Z. Tang, K. Zhang, S. Sun, Z. Gao, L. Zhang, Z. Yang, "An upper-limb power-assist exoskeleton using proportional myoelectric control", *Sensors (Basel), 10;14(4):6677-94*, 2014.
18. F. Di Nardo, C. Morbidoni, G. Mascia, F. Verdini, S. Fioretti, "Intra-subject approach for gait-event prediction by neural network interpretation of EMG signals", *BioMedical Engineering Online*, *19, 58*, 2020.

19. J. Rueterbories, E.G. Spaich, B. Larsen, O.K Andersen, "Methods for gait event detection and analysis in ambulatory systems", *Med. Eng. Phys, vol. 32, pp. 545-552,* 2010.
20. V. Agostini, G. Balestra, M. Knaflitz, "Segmentation and Classification of Gait Cycles*", IEEE Transactions on Neural Systems and Rehabilitation Engineering, vol. 22, NO. 5*, 2014.
21. H. Stolze, J. Ktuhtz-Bruschbeck, C. Mondwurf, A. Boczek-Funcke, K. Johnk, G. Deuschl, M Illert, "Gait analysis during treadmill and overground locomotion in children and adults", *Electroencephalography and Clinical Neurophysiology/Electromyography and Motor Control, vol. 105, pp. 490-497,* 1997.
22. P.O. Riley, G. Paolini, U. Della Croce, K.W. Paylo, D.C. Kerrigan, "A kinematic and kinetic comparison of overground and treadmill walking in healthy subjects", *Gait Posture, vol. 26, pp. 17-24,* 2014.
23. J. Song, J. Hidler, "Biomechanics of overground vs. treadmill walking in healthy individuals"*, Journal of Applied Physiology, vol. 104, pp. 747-755,* 2008.
24. B. Batlkham, C. Oyunaa, N. Odongua, "A Kinematic Comparison of Overground and Treadmill Walking", *Value in Health : the Journal of the International Society for Pharmacoeconomics and Outcomes Research, 17(7):A774*, 2014.
25. L. Wang, L. Cheng, G. Zhao, " Machine Learning for Human Motion Analysis: Theory and Practice", *Medical Information Science Reference, DOI: 10.4018/978-1-60566-900-7,* 2010.
26. Z. Tang, H. Yu, S. Cang, "Impact of load variation on joint angle estimation from surface emg signals", *IEEE Transactions on Industrial Electronics, vol. 63, pp 1923-1934,* 2016.
27. H. Alanazi, A. Abdullah, K. Qureshi, "A Critical Review for Developing Accurate and Dynamic Predictive Models Using Machine Learning Methods in Medicine and Health Care", *Journal of Medical Systems, vol. 41, pp. 1-10,* 2017.
28. L. Ying, F. Gao, H. Chen, and M. Xu, "Gait recognition based on Emg with different individuals and sample sizes", *2016 35th Chinese Control Conference (CCC)*, *pp. 4068-4072,* 2016.
29. C. Zhang, W. Peng, F. Peng, "Evaluation of sEMG-Based feature extraction and Effective Classification Method for Gait Phase Detection", *SpringerLink, Cognitive systems and signal processing, pp 138-149*, 2019.
30. R. Luo, S. Sun, X. Zhang, Z. Tang, W. Wang. "A low-cost End-to-End sEMG-based Gait Sub-phase Recognition System", *IEEE Transactions on Neural Systems and Rehabilitation Engineering*, *vol. 28, no. 1, pp. 267-276*, 2020.
31. J. Perry, "Gait Analysis: Normal and Pathological Function", *Slack Inc.: Thorofare, pp 9-130, NJ, USA*, 1992.
32. J.S. Kawalec, "Mechanical testing of foot and ankle implants", *Elizabeth Friis*, *Mechanical Testing of Orthopaedic Implants, Woodhead Publishing*, *pp. 231-253*, 2017.
33. T. Schmeltzpfenning, T. Brauner, "Foot biomechanics and gait", *in Woodhead Publishing Series in Textiles, Handbook of Footwear Design and Manufacture, pp. 27-48*, 2013.
34. M.B.I. Raez, M.S. Hussain, F. Mohd-Yasin. "Techniques of EMG signal analysis: detection, processing, classification and applications", *Biological procedures Online, vol. 8, pp. 11-35,* 2006.
35. M. Lindsay, S. Dwson, A. Harwell, R.Hopkins, J. Kaufmann, M. Master, P. Matern, K. Morrison-Graham, D. Quick, J. Runyeon, "Overview of Muscle Tissue", *Anatomy & Physiology, vol.10, pp. 549-602,* 2012.
36. H. Lodish, A. Berk, SL. Zipursky, "Myosin: The Actin Motor Protein"*, Molecular Cell Biology. 4th edition, Section 18.3,* 2000.
37. P. Konrad, "The ABC of EMG: A Practical Introduction to Kinesiological Electromyography", *in the ABC of EMG, Version 1.4, pp. 7-30, Noraxon INC. USA*, 2005.
38. S. Pham, Y. Puckett, "Physiology, Skeletal Muscle Contraction", *Treasure Island (FL): StatPearls*, 2021.

39. C.J. De Luca, “Surface electromyography: Detection and recording”, *DelSys Incorporated*, *pp. 1-10*, 2002.
40. G. De Luca, “Fondumental concepts in EMG signal acquisition”, *DelSys Incorporated*, *pp. 12-24*, 2003.
41. L. Wanhammar, “Filter Impulse Response: Digital Filters”, *In Academic Press Series in Engineerin*g, *DSP Integrated Circuits, pp. 115-186*, 1999.
42. T. D’Alessio, S. Conforto, “Extraction of the envelope from surface EMG signals”, *Journal of electromyography and kinesiology : official journal of the International Society of Electrophysiological Kinesiology, vol. 42, pp. 1-9,* 2001.
43. W. Rose, “Electromyogram Analysis”, *Mathematics and Signal Processing for Biomechanics*, *KAAP686, pp. 1-8*, 2011.
44. R. Schiavi, C. Frigo, A. Pedotti, “Electromyographic signals during gait: Criteria for envelope filtering and number of strides”, *Medical & Biological Engineering & Computing, vol. 36, pp. 171-178*, 1998.
45. A. Gulli, S. Pal, “Deep Learning with Keras: Implement neural networks with Keras on Theano and TensorFlow”, *Packt Publishing, Birmingham, Mumbai, pp. 9-189,* 2017.
46. IBM, “Neural Networks”, *ibm.com/cloud/learn/neural-networks*, Retrieved September 18, 2021.
47. D. Debanne, E. Campana, A. Bialowas, E. Carlier, G. Alcaraz, “Axon Physiology”, *Psychological Review, vol. 91, pp. 555-602*, 2011.
48. Y. Wang, “A New Concept using LSTM Neural Networks for Dynamic System Identification”, *American Control Conference (ACC)*, *pp. 5324-5329*, 2017.
49. Machine Learning Mastery, “A Gentle Introduction to Long Short-Term Memory Networks by the Experts”, *machinelearningmastery.com/gentle-introduction-long-short-term-memory-network-experts/*, Retrieved September 20, 2021.
50. F. Di Nardo, C. Morbidoni, A. Cucchiarelli, S. Fioretti, “Influence of EMG-signal processing and experimental set-up on prediction of gait events by neural networks”, *Biomedical Signal Processing and Control, 63:102232,* 2021.
51. C. Morbidoni, A. Cucchiarelli, V. Agostini, M. Knaflitz, S. Fioretti, F. Di Nardo, “Machine-Learning-Based Prediction of Gait Events from EMG in Cerebral Palsy Children”, *IEEE Transactions on neural systems and rehabilitation engineering, vol.29, pp. 819-830*, 2021.
52. H. Hermens. B. Freriks, C. Disselhorst-Klug, G. Rau, “Development of recommendations for SEMG sensors and sensor placement procedures”, *Journal of Electromyography and Kinesiology, vol. 10, pp. 361-374*, 2000.
53. D.F. Stegeman, H.J. Hermens, “Standards for surface electromyography: the European project “Surface EMG for non-invasive assessment of muscles (SENIAM)”, *Stegeman&Hermens*, *pp. 108-112*, 2007.
54. L. Mesin, R. Merletti, A. Rainoldi, “Surface EMG: The issue of electrode location”, *Journal of Electromyography and Kinesiology, vol. 19, pp. 719-726*, 2009.
55. F. Di Nardo, A. Mengarelli, E. Maranesi, L. Burattini, S. Fioretti, “Gender differences in the myoelectric activity of lower limb muscles in young healthy subjects during walking”, *Biomedical Signal Processing and Control, vol. 19, pp. 14-22,* 2015.
56. M.Z. Jamal, “Signal Acquisition Using Surface EMG and Circuit Design Considerations for Robotic Prosthesis”, *IntechOpen*, DOI: 10.5772/52556, 2012.
57. A. Gettami, J. Montelius, “An investigation of categorical variable encoding techniques in machine learning: binary versus one-hot and feature hashing”, *KTH Royal Institute of Technology School of Electrical Engineering and Computer Science, Cedric Seger*, *pp. 9-13*, 2018.
58. GitHub, “DeepEvent Version 0.4”, *github.com/LempereurMat/deepevent*, Retrieved April 5, 2021.

59. Machine Learning Mastery, “Loss and Loss Functions for Training Deep Learning Neural Networks”, *machinelearningmastery.com/loss-and-loss-functions-for-training-deep-learning-neural-networks/,* Retrieved September 20*,* 2021.
60. Machine Learning Mastery, “Gentle Introduction to the Adam Optimization Algorithm for Deep Learning”, *machinelearningmastery.com/adam-optimization-algorithm-for-deep-learning/*, Retrieved September 20, 2021.
61. S. Khandelwal, N. Wickstrasm, “Evaluation of the performance of accelerometer-based gait event detection algorithms in different real-world scenarios using the MAREA gait database”, *Gait Posture, vol. 51, pp. 84-90*, 2017.
62. D. Trojanello, A. Cereatti, U. Della Croce, “Accuracy, sensitivity and robustness of five different methods for the estimation of gait temporal parameters using a single inertial sensor mounted on the lower trunk”, *Gait Posture, vol. 40, pp. 487-492,* 2014.
63. D. Toledo-Pérez, M. Martinéz-Prado, R. Gomez-Loenzo, W. Paredes-Garcia, J. Rodirguez-Reséndiz, “A study of movement classification of the lower limb based on up to 4-EMG channels”, *Electronics*, *8, 259*, 2019.
64. J.H Ryu, D.H. Kim, “Multiple Gait Phase Recognition using Boosted Classifiers based on sEMG Signal and Classification Matrix”, *Proceedings of the 8th International Conference on Ubiquitous Information Management and Communication*, *vol. 90, pp. 1-4,* 2014.
65. Y. Ma, S. Xie, Y. Zhang, “A patient-specific EMG-driven neuromuscular model for the potential use of human-inspired gait rehabilitation robots”, *Computers in Biology and Medicine, vol. 70, pp. 88-98*, 2016.
66. A. Aia, H. Cheng, X. Lin, M. Omer, J.M. Atieno, “Survey of on-line control strategies of human-powered augmentation exoskeleton systems”, *Advances in Robotics & Automation, 05(03),* 2016.

Appendix

Fold 1	MAE (HS)	MAE (MS)	MAE(HR)	MAE (TO)	F1-Score(HS)	F1-Score(MS)	F1-Score(HR)	F1-Score(TO)
25	22.1	32.5	50.7	21.3	99%	100%	95%	100%
26	13.3	31.1	48.9	21.8	92%	97%	93%	97%
27	16.3	38.4	47.5	21.8	92%	96%	93%	98%
28	13.2	43.6	38.5	17.7	100%	100%	100%	100%
29	41.8	60.0	59.6	27.9	41%	77%	88%	99%
30	15.8	29.3	58.3	23.2	95%	98%	91%	99%
MV	17.9	41.5	50.4	22.4	88%	94%	93%	99%

Fold 1: Subjects 25, 26, 27, 28, 29 and 30 (Unseen Subjects). MAE (ms) and F1-Score related on each Unseen Subject. MV=Mean Average Value over the 6 subjects.

Fold 2	MAE (HS)	MAE (MS)	MAE(HR)	MAE (TO)	F1-Score(HS)	F1-Score(MS)	F1-Score(HR)	F1-Score(TO)
1	28.7	31.5	42.2	39.2	95%	98%	96%	95%
2	30.1	37.9	95.3	33.9	85%	90%	68%	88%
3	39.0	60.6	57.6	78.4	23%	83%	80%	59%
4	35.4	39.3	28.4	17.8	94%	98%	94%	97%
5	26.2	21.0	97.5	35.7	99%	100%	71%	97%
6	20.5	21.8	38.1	21.1	99%	99%	98%	100%
MV	28.5	34.1	54.1	32.3	89%	95%	86%	91%

Fold 2: Subjects 1, 2, 3, 4, 5 and 6 (Unseen Subjects). MAE (ms) and F1-Score related on each Unseen Subject. MV=Mean Average Value over the 6 subjects.

Fold 3	MAE (HS)	MAE (MS)	MAE(HR)	MAE (TO)	F1-Score(HS)	F1-Score(MS)	F1-Score(HR)	F1-Score(TO)
7	13.8	20.9	75.3	39.1	99%	100%	78%	99%
8	18.5	31.0	88.9	29.8	95%	92%	98%	95%
9	18.0	47.4	55.5	24.2	98%	96%	85%	99%
10	25.8	37.9	52.7	23.7	99%	95%	76%	94%
11	14.2	29.2	67.0	68.0	92%	98%	85%	94%
12	10.4	30.5	68.7	32.8	100%	96%	95%	99%
MV	16.1	33.2	65.2	34.3	98%	97%	85%	97%

Fold 3: Subjects 7, 8, 9, 10, 11 and 12 (Unseen Subjects). MAE (ms) and F1-Score related on each Unseen Subject. MV=Mean Average Value over the 6 subjects.

Fold 4	MAE (HS)	MAE (MS)	MAE(HR)	MAE (TO)	F1-Score(HS)	F1-Score(MS)	F1-Score(HR)	F1-Score(TO)
13	15.1	17.8	39.2	26.6	94%	91%	93%	92%
14	13.7	24.1	67.0	33.1	98%	95%	95%	99%
15	20.1	45.7	55.4	34.5	59%	88%	85%	97%
16	18.5	23.6	39.8	53.4	95%	99%	75%	90%
17	36.7	51.8	72.7	25.9	100%	95%	92%	99%
18	18.9	44.4	37.8	32.4	66%	100%	99%	99%
MV	21.4	34.1	55.0	34.1	89%	94%	89%	96%

Fold 4: Subjects 13, 14, 15, 16, 17 and 18 (Unseen Subjects). MAE (ms) and F1-Score related on each Unseen Subject. MV=Mean Average Value over the 6 subjects.

Fold 5	MAE (HS)	MAE (MS)	MAE(HR)	MAE (TO)	F1-Score(HS)	F1-Score(MS)	F1-Score(HR)	F1-Score(TO)
19	27.0	47.22	30.0	23.6	95%	98%	91%	96%
20	18.4	38.5	60.6	32.8	99%	99%	96%	100%
21	21.7	19.7	30.7	33.6	97%	99%	96%	97%
22	14.0	56.6	47.3	32.4	100%	83%	92%	98%
23	16.0	30.9	71.4	25.7	99%	100%	90%	99%
24	16.3	22.0	37.2	32.3	98%	100%	99%	100%
MV	19.4	32.5	44.1	30.2	98%	98%	94%	98%

Fold 5: Subjects 19, 20, 21, 22, 23 and 24 (Unseen Subjects). MAE (ms) and F1-Score related on each Unseen Subject. MV=Mean Average Value over the 6 subjects.